From the Kuiper Belt to Jupiter-Family Comets: The Spatial Distribution of Ecliptic Comets

Harold F. Levison

Space Science Department

Southwest Research Institute, Boulder, CO 80302

hal@gort.space.swri.edu

and

Martin J. Duncan

Department of Physics, Queen's University

Kingston, Ontario, Canada K7L 3N6

duncan@astro.queensu.ca

To Appear in *Icarus*

Abstract

We present numerical orbital integrations of thousands of massless particles as they evolve from Neptune-encountering orbits in the Kuiper belt for up to $1\,Gyr$ or until they either impact a massive body or are ejected from the solar system. The median dynamical lifetime of these objects is 4.5×10^7 years. We found that about 30% of these objects became visible comets. (We refer to a comet with perihelion distance $< 2.5\,AU$ as a 'visible' comet.) Of those, 99.7% were Jupiter-family comets (as defined by their Tisserand parameter, hereafter 'JFCs') when they first became visible, although some evolved out of the Jupiter family as time progressed. By comparing the observed orbital element distribution of JFCs to that produced by our simulations we deduce that JFCs are statistically most likely to have physical lifetimes of $\sim 12,000$ years. Based on this estimate of physical lifetimes and the fact that there are ~ 110 active, visible JFCs with $H_T < 9$, we conclude that there are currently $\sim 1.2 \times 10^7$ ecliptic comets (those with $T > 2$), of sizes consistent with this absolute magnitude, that originated in the Kuiper belt. This conclusion assumes that the rate of objects leaving the Kuiper belt has remained approximately constant over the history of the solar system. We calculate the orbital distribution of this population and show that $\sim 90\%$ are beyond the orbit of Neptune at any given time. In addition, we calculate the impact rates of these objects onto the planets. We find that a JFC impact onto Jupiter happens approximately once every 400 years and one on the Earth should occur once every 13 million years.

1. Introduction

In 1977, Kowal discovered the unusual object now known as (2060) Chiron (Kowal 1989), which is on an eccentric orbit that stretches from just inside the orbit of Saturn to just inside the orbit of Uranus. This object was the first discovered on an unstable planet-crossing orbit that lies entirely in the outer solar system. Since that time, a total of six objects on similar giant planet-crossing orbits have been discovered. These objects have come to be known as 'Centaurs' and, as many have suggested, probably represent the observational connection between the recently discovered trans-Neptunian Kuiper belt objects (Jewitt & Luu 1995, Cochran et al. 1995) and visible Jupiter-family comets.

Fernández (1980) first suggested that a belt of distant icy planetesimals could serve as the source of comets with periods less than 200 years. Duncan et al. (1988) strengthened this argument by performing dynamical simulations which showed that a cometary source beyond Neptune with a low initial inclination distribution (which they named the Kuiper belt) was far more consistent with the observed orbits of most of these comets than the randomly distributed inclinations of comets in the Oort cloud (see also Quinn et al. 1990). However, Duncan et al. (1988) and Quinn et al. (1990) started their simulations with objects that were already on unstable Neptune-encountering orbits. Torbett (1989) showed that chaos induced by planetary perturbations might transform some nearly circular orbits beyond Neptune into trajectories which can encounter Neptune – a suggestion which was later strengthened by Levison & Duncan (1993) and Holman & Wisdom (1993), who showed that this chaos was active on gigayear timescales.

In a previous paper (Duncan, Levison, & Budd 1995, hereafter DLB95), we followed the evolution of thousands of massless test particles in the Kuiper belt for times up to the age of the solar system. We showed that the Kuiper belt has a very complex structure that was formed due to the combined effects of mean-motion and secular resonances. For the purpose of this paper, the most important result in DLB95 was that there are many regions of the Kuiper belt in which the timescale for instability is on the order of the age of the solar system. In these regions the long-term dynamical erosion of particles is gradual enough for a significant fraction of the objects to survive the age of the solar system, while still being able to supply a large enough flux to explain the number of observed short-period comets.

This paper is therefore the culmination of research designed to construct a complete theory of the origin of the Jupiter-family comets (JFCs - as defined below) based on the Kuiper belt as their source region. Here we follow the dynamical evolution of particles once they leave the Kuiper belt and compare the resulting hypothetical population of visible comets with the population of observed comets.

Previous workers studying the dynamical transport of bodies from the outer to the inner planetary regions have been forced to use varying degrees of approximation in order to make the simulations computationally tractable. In an influential early study of the capture of comets from the Oort cloud, Everhart (1977) used a combination of tabulated single-planet scattering experiments together with Monte Carlo techniques to suggest that a fraction of near-parabolic orbits with perihelia as large as Neptune's orbit would be gravitationally scattered by the outer planets into orbits that are Jupiter–crossing and that a fraction of these would eventually become visible comets.

Later, Duncan et al. (1988) and Quinn et al. (1990) were forced for computational reasons to multiply the mass of each of the giant planets by factors of 10–40. The authors argued that since gravitational scattering is a diffusion process, this approximation should change the rate of evolution but not the statistical properties of the final distribution of orbits. (We shall show below that although this is qualitatively correct, some quantitative differences arise from more exact integrations). Furthermore, Wetherill (1991) and Fernández & Ip (1991) used an Öpik (1951) approximation with the correct planetary masses and obtained results very similar to Quinn et al (1990).

It has been clear for several years that an accurate prediction of the distribution of incoming comets from the Kuiper belt requires an extremely CPU–intensive direct integration with the correct masses of the planets and with the evolution of the planetary orbits also modeled more exactly. Direct integrations of the evolution of bodies on Chiron-like orbits have been performed for times up to 10^5 years (Scholl 1979, Oikawa and Everhart 1979, Hahn and Bailey 1990, Asher & Steel 1993) and for several other Centaur-like orbits for times up to 5×10^7 years by Dones et al. (1996). However, none of these integrations followed objects from the Kuiper belt until they were ejected from the solar system or impacted the Sun or a planet. In addition, none of them followed a large enough sample of particles for long enough periods to map out statistically the distribution of Centaurs and ecliptic comets throughout the solar system.

This paper presents the results of gigayear integrations of comets originating in the Kuiper belt. Our calculations have allowed us to calculate the current orbital element distribution of the bodies in transition (which are most likely the Centaurs) as well as determine some limits on the active lifetime of JFCs. Before proceeding, we briefly summarize the terminology we have adopted in classifying comets.

For historical reasons, comet taxonomy has until recently been based largely on orbital period: long-period comets were those with periods greater than 200 years, short-period comets had periods less than 200 years, with the latter group sometimes being subdivided into the Jupiter family (periods less than 20 years) and the Halley type (periods between 20 and 200 years; also occasionally referred to as intermediate-period comets). This taxonomy was long recognized as being arbitrary. In our numerical integrations of all of the known short-period comets (Levison & Duncan 1994 ; hereafter called LD94) we found that most comets move between Jupiter-family and Halley-type comets (hereafter HTCs), as defined above, many times in their dynamical lifetimes. However, it was found that the Tisserand parameter with respect to Jupiter,

$$T = \frac{a_J}{a} + 2\sqrt{(1-e^2)\frac{a}{a_J}}\ \cos i,$$

did not vary substantially during our integrations, where a, e, and i are the semi-major axis, eccentricity, and inclination of the comet, respectively, and a_J is the semi-major axis of Jupiter. [1] This suggests that a comet classification scheme based on the Tisserand parameter, as first suggested by Carusi & Valsecchi (1987), may be more appropriate.

In view of the deficiencies of the old classification based on period, we adopt here a new comet taxonomy using the Tisserand parameter, based on that proposed by one of us (Levison 1996). Bodies on orbits with $T > 2$ are called *ecliptic* comets unless they are in trans-Neptunian orbits which are stable on timescales comparable to or larger than the age of the solar system. (This is a slight refinement on the original scheme in Levison 1996, in which Kuiper belt objects would also be classified as ecliptic comets. In this work it is important to be able to distinguish between stable Kuiper belt objects and comets on unstable orbits.) Those with $T < 2$ (which are mainly from the Oort cloud) are called *nearly isotropic* comets.

---

[1] For the remainder of this paper, T refers to the Tisserand parameter with respect to Jupiter. The Tisserand parameters with respect to the other planets are T_S, T_U, and T_N for Saturn, Uranus, and Neptune, respectively. In addition, the Tisserand parameter with respect to an arbitrary planet is represented by T_p.

Ecliptic comets can be further subdivided into three groups. Comets with $2 < T < 3$ can experience low-velocity encounters with Jupiter and thus can be dynamically dominated by that planet. Following Levison (1996), we call comets with T in this range *Jupiter-family* comets, usually abbreviated as JFCs. This class has most of the same members as the Jupiter family defined by the orbital period. Comets with $T > 3$ (which cannot cross Jupiter's orbit) should not be considered members of the Jupiter family. A comet that has $T > 3$ and $a < a_J$ is designated an *Encke-type*. Note that this combination of the T and a implies that the orbit of such an object is entirely interior to Jupiter, i.e., the aphelion distance is less than a_J (assuming the orbit of Jupiter is circular). A comet that has $T > 3$ and $a > a_J$ (orbit is exterior to Jupiter) is designated a *Chiron-type*. It is important to note that Chiron-type comets are probably the same as Centaurs. The differences between an asteroid and a comet in this part of the solar system are not clear.

Finally, as with any model, a comparison must be made between the results of our simulations and observations. To perform such a comparison, we must correct for observational selection effects. A complete analysis is beyond the scope of this paper. Thus, we adopt the convention developed by Duncan et al. (1988) and used in LD94, which assumes that all active Jupiter-family comets with $q < 2.5\,AU$ have been discovered, while all with $q > 2.5\,AU$ have not. For the remainder of this paper, we refer to comets with $q < 2.5\,AU$ as *visible* comets. Clearly, the assumption that all JFCs with $q < 2.5\,AU$ have been discovered is not correct, because several have been discovered in the last few years (see Fernández et al. 1992). We attempt to compensate for the incompleteness in Section 4. However, it should be noted that in this paper this assumption plays a role only in the determination of total numbers of comets and not in the shape of the distributions that we calculate. Thus, there is an undetermined scale factor of order unity that may have to be applied to some of our results when a better estimate of the completeness of the JFCs is available.

In addition, our numbers are best interpreted as applying to the fraction of comets with sizes above an effective lower limit which is as yet unknown.

With these definitions and assumptions as background we are ready to proceed. In Section 2, we discuss the numerical methods and initial conditions used in these calculations. In Section 3 the major results of the simulation are presented. We use the results of Section 3 in Section 4 to estimate the physical lifetimes of JFCs and the total number of ecliptic comets. In Section 5, we predict the impact and close encounter rates with the planets, while in Section 6 we present our conclusions.

2. Numerical Methods and Initial Conditions

As part of DLB95, we followed the orbital evolution of 1300 test particles within the Kuiper belt which had initial orbits with low to moderate eccentricity (0.01 – 0.3) and inclinations of one degree for times up to 4 billion years – essentially the age of the solar system. In Figure 1, we plot the inclination of objects as they left the Kuiper belt (i.e., first had a strong encounter with Neptune) as a function of their initial semi-major axes. Only objects that left the Kuiper belt after being stable for over a billion years are included in this plot. Therefore, the orbits of these particles are most likely representative of the orbits of objects currently leaving the Kuiper belt. Thus, they provide representative initial conditions for the current calculations.

In Figure 1, the symbols represent different initial eccentricities in the DLB95 calculation. Members of this population with initial $e \lesssim 0.1$ arise in a region between 34 and 42 AU and typically have inclinations less than 10°as they leave the belt. A small fraction, which can have inclinations as high as 15°, are those leaking from Neptune's 2:3 mean motion resonance. Objects in DLB95 with initial eccentricities between 0.1 and 0.2 (shown as filled symbols in Figure 1) typically originate from two regions – a band between 42 and 50 AU and a zone inside of 40 AU of narrow bands centered on the low-order mean motion resonances. Objects originating in the outer region have final inclinations $\lesssim 10°$. Objects originating in the zone inside of 40 AU with $e > 0.1$ can have surprisingly large inclinations – as large as 25°.

We chose 20 particles in Figure 1 as our initial conditions for the calculations reported in this paper. These particles are marked by the gray circles in the figure. In general, we chose all the particles with initial eccentricities of 0.05, since the real nonresonant Kuiper belt objects have eccentricities that typically range from

0 to 0.1. Our chosen particles have inclinations that range from near 0 to 16° at the time of their first encounter with Neptune. In addition, we included two particles that were initially in the 2:3 mean motion resonance that left the Kuiper belt with inclinations $\sim 24°$. Since it seems unlikely that objects with such high inclinations are common in the Kuiper belt, we will study the evolution of such particles as special cases and they will not be included in the general description of the resulting Centaur and Jupiter-family comet populations.

Each of our chosen particles had to be integrated in separate runs, since they all left the Kuiper belt at different times and thus the planets were in different locations. Each particle was cloned 99 times or 149 times depending on the speed of the computer on which the run was performed. The cloning involved adding a uniformally distributed random number between $\pm 1 \times 10^{-7}\,AU$ to each of the positional coordinates of the particle. The orbits of the clones were integrated under the gravitational influence of the Sun and the four giant planets by using the $RMVS$ integration scheme developed in LD94. Our integration scheme is based on the method of Wisdom & Holman (1991), but additionally it can handle close encounters between particles and planets. The effects of the terrestrial planets and nongravitational forces were not included. In all, the orbits of 2200 particles were integrated.

The trajectory of a particle was followed for 10^9 years unless it was ejected from the solar system, impacted the Sun or a planet, or reached a semi-major axis of $1000\,AU$. We stopped following a particle at $a = 1000\,AU$ because galactic tides and passing stars begin to have significant dynamical effects at this distance (Duncan et al. 1987). Presumably, most of these objects will eventually become part of the Oort cloud or be ejected from the solar system. In order to better study the resulting population of Jupiter-family comets, a particle was cloned nine times the first time it reached a perihelion distance less than $2.5\,AU$.

3. Simulation Results

3.1 The Origin of Jupiter-Family Comets

As discussed in §1, the main purpose of this research is to finish a complete simulation of the formation of Jupiter-family comets (JFCs). The outcome of such a simulation must reproduce the orbital element distribution of the Jupiter family, which is shown in Figures 2A and 2B. Figure 2A shows the distribution of known comets' semi-major axes, a, as a function of their Tisserand parameters with respect to Jupiter, T. The dashed lines show the range of the Jupiter family: $2 < T < 3$. Objects above the solid curve must have perihelion distances, q, greater than $2.5\,AU$. These objects are more difficult to discover and thus the lack of objects above the solid curve is mostly due to observational biases. Note that most JFCs have $2.5 \lesssim T \lesssim 3$ and $3 < a < 4.5\,AU$.

In order to compare the results of our simulations to the distribution of real comets, Figures 2C and 2D show the orbital element distribution of all visible ($q < 2.5\,AU$) comets in our simulation when they first become visible. When making a comparison between the real and simulated JFCs in Figure 2 it is important to note that there are about five times as many points in the simulated population as in the observed population. Thus, outlying data points in the simulated population are less significant than they may otherwise seem. The distribution of comets in our simulation matches that for the real Jupiter family remarkably well (a quantitative comparison will be performed in §4). Therefore, our simulations show that the Kuiper belt is an excellent source for the Jupiter-family comets. However, the Kuiper belt does not produce very many Halley-type comets (at least initially, see §3.3). This result is consistent with the results of earlier work (Quinn et al. 1990) that concluded that the Kuiper belt is the main source of JFCs and that the Oort cloud is the most likely source for most of the Halley-type comets.

One of the most interesting aspects of the distributions shown in Figure 2 is the very narrow range in T that Jupiter-family comets occupy. Although we define a Jupiter-family comet as one with $2 < T < 3$, the median T for the family is 2.8. The narrow range in T is related to the flat inclination distribution seen for these comets: an object on a Jupiter-crossing orbit with $T > 2.8$ and $q < 2.5AU$ must have an inclination less than $\sim 26°$.

The following question naturally arises: Why do JFCs have such a narrow range in T? Interestingly, this appears to be due to the fact that as objects leave the Kuiper belt, they have Tisserand parameters with respect to Neptune, T_N, that are near 3. A simple illustration demonstrates this effect. Assume that the solar system is planar and that the Tisserand parameter with respect to a given planet is roughly conserved while an object's dynamics are dominated by that planet. A good example of an object leaving the Kuiper belt is one initially trapped in the 2:3 mean motion resonance with Neptune. For illustrative purposes, we choose an object with $a = 39.4\,AU$ and $e = 0.25$. This object has $T_N = 2.98$. Since T_N is nearly conserved as the object interacts with Neptune, the smallest perihelion distance to which Neptune can scatter this object is $q = 17.7\,AU$, just enough to become a Uranus-crosser. In this orbit, the particle has $T_U = 2.86$. As a result, the smallest q orbit that Uranus can scatter the particle onto is $q = 9.0\,AU$, barely a Saturn-crosser. The particle now has $T_S = 2.94$ and thus Saturn can lower its q to only $3.8\,AU$. So, Saturn cannot by itself scatter objects onto visible orbits. This is the main reason why the Kuiper belt does not produce many Halley-type comets. With $q = 3.8\,AU$, the particle in our example has a Tisserand parameter with respect to Jupiter of $T = 2.82$. It is interesting to note that both Kazimirchak-Polonskaya (1972) and Everhart (1977) speculated that this type of handoff between the planets is responsible for the capture of low-inclination near-parabolic comets from the Oort cloud. Although Quinn et al. (1990) showed that this mechanism is not very important for most Oort cloud comets, our results show that it is indeed important for objects that originate in the Kuiper belt.

The evolution of a representative particle originating in the Kuiper belt that becomes a visible comet is shown in Figure 3. Figure 3a shows the Tisserand parameter of this particle with respect to each giant planet (blue is Jupiter, red is Saturn, green is Uranus, and black is Neptune) as a function of time. A circle of the appropriate color is used if the comet's orbit crosses that of a given planet: a colored dashed line is used otherwise. The Tisserand parameter with respect to a planet is always observed to be larger than 2.8 and usually larger than 3, at which point the particle is not crossing the planet. Notice that we find that when the particle is crossing the orbit of a planet, the Tisserand parameter with respect to that planet is always near 3.

Figure 3b shows the locations of the particle's orbit in the q–Q (perihelion-aphelion) plane. The positions are joined by blue lines until the particle first became 'visible' ($q < 2.5\,AU$) and are linked in red thereafter. Initially, the particle spent considerable time with perihelion near the orbit of Neptune and aphelion well beyond the planetary system. However, once its perihelion dropped to Uranus' location, this particle, which was chosen at random from our integrations, clearly shows the handoff behavior described above. It evolved at relatively small eccentricity to visibility (cf. the lines of constant eccentricity e =0.2 and 0.3 on the figure) and it spent considerable time with perihelia near the semi-major axes of one of the three outer planets. Its post-visibility phase is reasonably typical of Jupiter-family comets, as the discussion in §3.4 shows.

The simple handoff argument outlined above not only predicts that all JFCs should have $T \sim 3$, but also predicts that if a particle is crossing the orbit of a planet, it will have a Tisserand parameter *with respect to that planet* that is near

3. Indeed, we observe this behavior in our integrations. The median Tisserand parameter with respect to a planet of all particles that cross its orbit ranges from 2.6 to 2.8 in the outer solar system. One interesting consequence of this behavior is that since $T \sim 3$ precludes high-inclination orbits, then under the assumption of the approximate conservation of T, none of the outer planets can pump up the inclination of the Kuiper belt objects as they migrate through the planetary system. This is illustrated in Figure 4, which shows a plot of the mean cosine of the inclination as a function of perihelion distance. Note that the inclinations are small everywhere. (Recall that $\cos(i) = 0.95$ corresponds to an inclination of 18°.) In addition, much of the structure seen in the figure is due to the narrow range of T at each planet. Note that there is a significant dip in inclination just outside the orbit of each planet. For a given value of T near 3, the relationship between the maximum inclination that a particle can have and its perihelion distance forces the inclination to be small if q is small. Thus, in order for a planet to scatter a comet down to the planet interior to it, the inclination of the comet must be smaller than average.

Another very important implication of the results outlined in the previous few paragraphs is that Kuiper belt objects will tend to have a fairly predictable evolution as they migrate inward. They will usually be under the control of one planet. The planet will scatter them inward and outward in a random walk, eventually handing them off to the planet directly interior or exterior to it. Thus, the eccentricities of comets between the planets and before reaching visibility will remain relatively small, $e \sim 0.2$. This trend is observed in our simulations (cf. Figure 3b and §3.4).

It is clear that the above scenario is only part, although a very important part, of the picture. Over 60% of the particles in our integrations do not become visible comets. The vast majority of these objects have to evolve onto orbits that have T with respect to one of the planets that is significantly less than 3. One mechanism to accomplish this can again be illustrated in a planar solar system. In the above example, the comet is handed to Uranus with $T_U = 2.86$. Although Uranus cannot eject this object, it could put it on an orbit with $a = 180\,AU$, which is a Neptune-crosser. For such an orbit, $T_N = 2.4$, which is small enough to ruin the narrow range of T and flat inclination distribution observed in the visible JFCs. This situation would worsen if the comet were handed back and forth several times.

So, why do objects that have $T_p \ll 3$ apparently play so small a role in the distribution of ecliptic comets? The answer to this puzzle appears to be that a comet with small T with respect to a planet is more likely to be ejected from the solar system by that planet than a comet with T closer to 3. A parabolic orbit has $T_p = 2\sqrt{2q/a_p}\cos i$, where q and i are the comet's perihelion distance and inclination, respectively, and a_p is the semi-major axis of the planet. The particle's perihelion distance must satisfy $q \leq a_p$ for an ejection, which implies that $T_p \leq 2\sqrt{2} \approx 2.83$. Particles with $T_p > 2\sqrt{2}$ cannot be ejected by a planet. In addition, the closer a particle's T_p is to $2\sqrt{2}$ the more difficult it is for a planet to eject it. The solid angle of the loss cone for objects ejected from the solar system by an encounter with a planet is

$$4\pi\left(\frac{1}{2} - \frac{T_p - 2}{4\sqrt{3 - T_p}}\right),$$

which is approximately 5.5 steradians (44% of a sphere) for our above example of $T_p = 2.4$. So, if a comet did follow an evolutionary path that decreased its Tisserand parameter, it would be much less likely to survive to become a visible JFC.

The argument presented in the last paragraph implies that there should be a correlation between a comet's initial T with respect to Neptune and the probability that it becomes a visible JFC. We see this correlation in our integrations. Figure 5A shows the fraction of objects that become visible JFCs as a function of their initial T_N. Recall that at least 100 particles in our simulations were clones of an individual particle. Thus, these 100 particles had, for the most part, the same initial orbit. Each dot in Figure 5 represents a group of particles that had the same initial orbit. Note that the fraction of objects that become visible JFCs is smaller for objects that had smaller T_N, as expected from the above argument.

The initial inclinations of our objects ranged from under $1°$ to about $24°$. It is interesting (and gratifying) that the orbital properties of the JFCs resulting from each of these particles do not seem to be strongly correlated with the particle's initial Kuiper belt orbit. This is illustrated in Figures 5B and 5C. In Figure 5B, we plot the mean $\cos(i)$ of particles in a group when they first become visible as a function of the cosine of their initial inclination. In Figure 5C, we plot the mean Tisserand parameter with respect to Jupiter (T) of a group of particles when they first become visible as a function of their initial Tisserand parameter with respect to Neptune (T_N). As can be seen in these figures, no correlation exists. Thus, we can conclude that a comet that becomes a visible JFC forgets the details of its original orbit and the orbital element distribution of JFCs is not sensitive to the assumed initial Kuiper belt orbits. We make use of this result in §4, where we estimate the physical lifetimes of comets.

3.2 The Fates of Objects Leaving the Kuiper Belt

We now explore some statistics of our runs. The median dynamical lifetime of objects in our runs is 4.5×10^7 years, while 10% of the particles survived for 4.3×10^8 years. Of the 2000 test particles in our main runs, 628 (31%) became visible comets, all but two of which were JFCs. Of the remainder, 25% were ejected from the solar system and 68% reached $a > 1000\,AU$. The vast majority of the latter particles are presumably either ejected at a later time or become part of the Oort cloud (cf. Duncan, Quinn and Tremaine 1987). About 1.5% of our particles impacted a planet before they became visible or were ejected. Most hit either Uranus or Neptune: about 30% hit Neptune, 33% impacted Uranus, 13% hit Saturn, and 23%

impacted Jupiter on the way in. Also about 5% of the particles survived the length of the integration, 10^9 years. All of the survivors had semi-major axes outside the orbit of Neptune.

Of the 628 particles that became visible, 97% were eventually either ejected from the solar system or reached $a > 1000\,AU$. Approximately 2% impacted Jupiter and 0.3% impacted Saturn. None of these objects hit Uranus or Neptune. (Recall that the terrestrial planets were not included in these calculations.)

Only $\sim 1\%$ of the objects that became visible eventually became sun-grazers. This is surprising since in LD94 we found that $\sim 6\%$ of the known short-period comets became sun-grazers. Part of the discrepancy between the calculations presented here and those of LD94 is due to that fact that in LD94 we did not differentiate between JFCs and Halley-type comets ($T < 2$, $a < 40\,AU$) when considering sun-grazers. Re-evaluating our previous integrations, we find that half of the objects that became sun-grazers were Halley type, although HTCs represented only $\sim 10\%$ of the comets integrated in LD94. Indeed, we find that a full 30% of the Halley-type comets became sun-grazers, while only 3% of the JFCs shared the same fate in LD94. Another slight discrepancy between the two calculations is found when considering the median dynamical lifetimes. In LD94 we found that the mean dynamical lifetime of these objects is 3.3×10^5 years while here we are finding it to be 2.7×10^5 years.

We believe that these differences are due to the fact that in LD94, we included three of the four terrestrial planets (Mercury excluded), while they were not included in the present calculation. Rare encounters with the terrestrial planets will tend to decouple a comet from Jupiter, thus increasing its lifetime and perhaps increasing the probability that secular effects will drive it into the Sun. Unfortunately, including the terrestrial planets in the present set of calculations was not practical, because it was necessary to integrate for 10^9 years, while in LD94 we integrated for only 10^7 years.

3.3 The Kuiper Belt as the Source of Halley-Type Comets

As discussed above, Figure 2 shows that the Kuiper belt does not produce many Halley-type comets, at least initially. Indeed, of the 628 comets that became visible in our integrations, only one was clearly an HTC when it first became visible. This is consistent with the earlier work of Quinn et al. (1990) and it led them to conclude that most HTCs must originate in the Oort cloud.

The analysis of our integrations of the orbits of the comets presented in LD94 seems to support the idea that HTCs come from the Oort cloud. We found that comets do not move between the Jupiter family and Halley type very often: less than 8% of comets changed classes during the integration, and most of those that did tended to remain near the $T = 2$ dividing line throughout. Less than 2% of the comets switched from $T > 2.5$ to $T < 1.5$. The integrations presented here are consistent with those of LD94. Indeed, here we find that a smaller fraction of comets change class after they first become visible — 3% and 0.8%, respectively. Presumably this difference is due to the lack of terrestrial planets and the fact that the LD94 simulation included Oort cloud comets.

However, in the current set of integrations, we find that the dynamical lifetimes of objects that move from the Jupiter family to the Halley type are much larger than those that remain JFCs (an analysis that we did not perform in LD94). Indeed, objects that evolved from $T > 2.5$ to $T < 1.5$ have a median dynamical lifetime after becoming visible of 1.3×10^6 years compared to only 2.7×10^5 years for the population as a whole. So, although few objects make the transition from a visible JFC to a visible HTC, these objects can potentially be overrepresented in the observed population of comets because of their long lifetimes. Indeed, we find that in a snapshot of the population of comets produced in our simulation of objects leaving the Kuiper belt, 13% of all visible comets with $a < 40\,AU$ will be HTCs.

Interestingly, 13% of the known visible comets with $a < 40\,AU$ are also HTCs.

Can we therefore conclude that most HTCs also originate in the Kuiper belt? A further analysis shows that this is likely not the case for two reasons: *i*) The orbital element distribution of the HTCs produced in our simulation is significantly different than that observed in nature. In the observed population of HTCs, 38% have $T < 1$, while in our simulations only 2% have $T < 1$. In addition, all of the retrograde comets in the observed population have $T < 0$, but none of our simulated comets do. This is due to the fact that all the observed retrograde comets have $a > 7\,AU$, while all of the retrograde test particles in our simulation have $a < 6\,AU$. *ii*) A'Hearn et al. (1995) have recently shown that JFCs and HTCs on average have different coma carbon abundances. Since the HTCs produced in our simulation are derived from the same source as our JFCs, we would not expect any such differences. Therefore, the HTCs that are produced in our simulation are unlike most of the observed HTCs.

There are two ways of reconciling the observations and the integrations. First, although we find above that both our simulations and the observations agree that 13% of visible comets are HTCs, this is most likely a coincidence. As discussed in §3.1, when calculating the fraction of HTCs in our simulations, we assumed that the population was complete to $q = 2.5\,AU$. This assumption is clearly in error for the observed HTCs. Of the 21 known HTCs, all have $q < 2\,AU$. Therefore, if the sample were complete to $q = 2.5\,AU$, the observed fraction of comets that are HTCs would be significantly larger. Thus, we clearly need another source for HTCs. Second, as discussed above, the vast majority of objects that become visible HTCs in our simulations are first visible JFCs. We find that it takes at least 10^5 years and usually over 10^6 years to become a visible HTC after the comet first becomes visible as a JFC. During that time it is likely that many of these comets will become extinct before the transition is accomplished. (We discuss the physical lifetimes of comets in detail in §4.) So it is likely that very few of these objects contribute to the observed population of active comets. For both of these reasons, we conclude that not all HTCs originated in the Kuiper belt. In addition, we believe, because of the compositional results of A'Hearn et al. (1995), that the physical lifetime argument is very important and thus that very few of the active HTCs originated in the Kuiper belt.

3.4 The Spatial Distribution of Ecliptic Comets

Figure 6 shows the distribution of the ecliptic comets (as defined in §1) derived from our simulations, assuming that the rate of objects leaving the Kuiper belt has remained approximately constant over the last $\sim 10^8$ years and that there was no huge influx at early epochs. The figure is a contour plot of the fraction of comets per square AU in perihelion-aphelion (q–Q) space. The figure was generated by binning the q–Q values of all the comets at all output points in the integrations, which occurred once every 10^4 years before a comet became visible and once every 1000 years after it became visible. The resulting matrix was then normalized so that the total number is one. It is important to note that the contours are not in terms of the surface density in physical space, but in q–Q space. Also shown in the figure are curves of constant eccentricity and semi-major axis.

There are two well-defined regions in Figure 6. Beyond approximately $Q = 7\,AU$, we see a ridge of high density extending diagonally from the upper right to the center of the plot, near $e \approx 0.25$. The peak of this ridge is near $e = 0.2$ at large Q and tends to increase to $e \approx 0.3$ near $Q \sim 7\,AU$. As we discussed in §3.1, we expect the eccentricities of objects that are between the planets and not yet under Jupiter's control to be about 0.25 due to the constraints of the Tisserand parameter. The peak density in this ridge drops by almost two orders of magnitude as it moves inward, having a minimum where the semi-major axes of the comets are the same as Jupiter's. This population extends inward of Jupiter's orbit and terminates near the 2:1 mean motion resonance with Jupiter. Indeed, we find that objects can be forced onto nearly circular orbits with semi-major axes as small as $\sim 4\,AU$. This inner edge is coincident with the inner edge of Jupiter's 'crossing zone' at $3.88\,AU$. Gladman & Duncan (1990) defined Jupiter's 'crossing zone' as the region in which objects on initially circular orbits can become Jupiter-crossing. Since this process is time reversible, it is not then surprising that Jupiter can drive comets into nearly circular orbits in this region.

Inside of $Q \approx 7\,AU$ the character of the distribution is quite different. Here there is a ridge of high density extending vertically in the figure at $Q \sim$ 5–6 AU that extends over a wide range of perihelion distances. Objects in this region are the Jupiter-family comets. This characteristic of a very narrow distribution in Q is seen in the real JFCs and is again a result of the narrow range in T.

There is also a population of objects that have perihelia that are fairly smoothly distributed throughout the outer solar system which also have aphelia that lie well beyond the planets. We discuss this 'scattered disk' below.

Superimposed on the smooth distributions discussed above are several small local variations that, although not very important in terms of the number of objects in them, are of dynamical interest because they illustrate the possible dynamical paths that objects can take. The one marked by the symbol '1:2' in Figure 6 is caused by the 1:2 mean motion resonance with Neptune. Figure 7 shows the behavior of a particle that enters this region. This particle is initially in a nonresonant, Neptune-crossing orbit. It successively becomes trapped in and then escapes from Neptune's 3:4 and 3:5 mean motion resonances. Finally, it gets trapped in the 1:2 mean motion resonance with Neptune, where it stays for the remainder of the integration. In this case we extended the integration to 2 billion years. Notice that there are phases when the particle's eccentricity becomes very small ($q \to a$) when it is in a given resonance. Indeed, at $t = 1.54 \times 10^9$ years, this particle has

$e = 0.0003$! Therefore, it is possible for mean motion resonances to force objects into nearly circular orbits. However, this type of behavior is rare — of the 2200 particles that we integrated, only three were driven to small eccentricities by mean motion resonances while outside the orbit of Neptune. It is important to note that they all had $i \gtrsim 15°$ while their eccentricities were small, since in DLB95 we showed that low-inclination, nearly-circular orbits in the 1:2 mean motion resonance with Neptune are stable.

In the lower right of Figure 6, we see faint indications of populations of what historically have been called Saturn-family, Uranus-family, and Neptune-family comets, i.e., comets with $Q \sim 10\,AU$, $Q \sim 20\,AU$, and $Q \sim 30\,AU$, respectively. These can be seen as faint vertical ridges at $q \lesssim 1\,AU$ for these aphelion distances. Comets in these peaks have $T < 2$ and thus are examples of the Halley-type comets discussed in §3.3. As discussed above, all of the comets within these peaks first went through a phase when they were visible JFCs. Therefore, these structures are formed by comets moving outward through the solar system. Objects moving in from the Kuiper belt rarely have eccentricities this large. This dichotomy in eccentricity is also seen in the pre- and post-visibility trajectories for the particle plotted in Figure 3b.

The gray dot in Figure 6 shows the location of the unusual comet 2P/Encke. 2P/Encke is on an orbit that is completely decoupled from the giant planets, since $Q = 4.09\,AU$. (See LD94 for a complete discussion of the dynamics of this comet.) Surprisingly, we have not been able to create this comet in our simulations. There are four possible explanations for this: i) The dynamical mechanism that creates comets similar to 2P/Encke requires interactions involving the terrestrial planets, which are not included in these simulations. ii) Comets similar to 2P/Encke are very rare and thus none of our particles happened to follow that path. Recall that we integrated the orbits of only a few thousand objects. The real solar system has a significantly greater number of objects to deal with. *iii*) 2P/Encke did not originate in the Kuiper belt, but perhaps originated in the Oort cloud, the outer asteroid belt, or the Trojan swarm of Jupiter. *iv*) The dynamical mechanism that creates comets similar to 2P/Encke requires nongravitational forces which were not included in our simulations. It remains to be determined which of these explanations is correct, although we tend to favor explanation (*iv*).

Figure 8 shows the time-averaged surface density distribution of ecliptic comets normalized to a total number of one. Surprisingly, 90% of the comets are beyond the orbit of Neptune. This is due to the fact that most particles spend a most of their time beyond Neptune *after* they first encounter it: the median amount of time that an objects spends with $a > 30\,AU$ after it first becomes a Neptune-crosser is 3.6×10^7 years, which can be compared to the median total dynamical lifetime of 4.5×10^7 years.

The surface density distribution shown in Figure 8 is fit well by a power law of the form $\Sigma = \Sigma_0\, r^{-\alpha}$ outside of $30\,AU$ and inside of $\sim 8\,AU$, where r is heliocentric distance. In the inner regions $\alpha \approx 1.3$. Beyond $30\,AU$, $\alpha \approx -2.8$, close to the value of -2.5 expected for the steady-state distribution of bodies diffusing outward in semi-major axis with nearly constant perihelia close to Neptune (Yabushita 1980; Duncan et al. 1987). The much steeper dropoff beyond $\sim 1000\,AU$ is an artifact, since we remove particles with aphelia beyond $2000\,AU$. Galactic tides and passing stars begin to have significant dynamical effects at distances of a few thousand AU (cf. Duncan et al. 1987), so our dynamical model is no longer valid at those distances.

It is important to note that our current simulations begin with objects that have come within the Hill sphere of Neptune. Therefore, the distribution shown in Figure 8 does not show the primordial Kuiper belt, which extends from $\sim 34\,AU$ outward (Duncan et al. 1995). We estimate that the Kuiper belt contains between three and four orders of magnitude more objects than the distribution in Figure 8. This estimate is discussed in detail in the next section.

Finally, it is also important to note that the distributions shown in Figures 6 and 8 assume a constant rate of influx from the Kuiper belt for the last $\sim 10^8$ years and no huge influx at early epochs. The latter assumption is in some doubt since there is mounting evidence that the Kuiper belt was very massive at early epochs (see Stern 1995 or Levison et al. 1996b for a discussion of this). Recall that about 5% of the particles survived the length of the integration (10^9 years). All of the survivors had semi-major axes outside the orbit of Neptune. This implies that if the primordial Kuiper belt were indeed massive, there may be a significant population of objects with highly eccentric orbits in an extended disk beyond the orbit of Neptune. Indeed, the density in this disk could be an order of magnitude larger than the distribution shown in Figure 8. We will address the issues raised by this 'scattered' Kuiper belt in a future paper.

4. Physical Lifetime of JFCs and the Total Number of Ecliptic Comets

Using the integration in the last section, it is possible to determine, or at least constrain, the physical lifetimes of JFCs as well as the ratio of extinct to active comets in the solar system. In this section, we present two measures of these parameters based on the evolution of comets after they first become visible JFCs.

In LD94, we showed that the inclination distribution of the Jupiter family puffs up as a function of time. Given that we know the inclination distribution of the JFCs in our simulation as a function of time, we can estimate the activity lifetime of comets by comparing the inclination distribution of the observed JFCs with the integrations in what follows. (We note that the following is similar to the arguments we presented in LD94. However, the current argument is much simpler because here we know the inclination distribution of the JFCs when they first become visible.)

Define τ as the age of a visible JFC. By this we mean the length of time since the comet was *first* injected into an orbit with $q < 2.5AU$ and $2 < T < 3$. Define $\zeta(i,\tau)$ as the number of comets in the visible Jupiter family with inclinations between i and $i + di$ and with ages between τ and $\tau + d\tau$. If there were no physical aging and comets did not become extinct, then the observed inclination distribution would be

$$\xi(i) = \int_0^\infty \zeta(i,\tau)\, d\tau. \tag{1}$$

Note that in the situation where comets do become extinct then $\xi(i)$ is the current inclination distribution of both the active and extinct JFCs with $q \leq 2.5AU$. If we model the effects of physical aging by *assuming* that all comets remain active for t_f years (after which they are permanently extinct), then the inclination distribution of the active visible JFCs is

$$\xi_{active}(i) = \int_0^{t_f} \zeta(i,\tau)\, d\tau. \tag{2}$$

The distribution, $\zeta(i,\tau)$, can be directly determined from our integrations, and thus we can easily calculate both $\xi(i)$ and $\xi_{active}(i)$. In Figure 9A, we compare the results of these calculations with the inclination distribution of observed visible JFCs. In the figure, we plot the fraction of objects with inclinations less than i for the observed comets (bold curve) and for our simulated JFCs for three values of t_f: $t_f = 0,\ 10^4$ years, and 4×10^4 years. First notice that the distribution of observed comets and that of our simulated comets when they first become visible are distinctly different. Indeed, a Kolmogorov-Smirnov test shows that the probability that the two distributions are derived from the same parent distribution is 7×10^{-3}. However, for values of $t_f \approx 10^4$ years the distributions match fairly well (see below).

This type of analysis can be performed on another dynamical measure of t_f. We find in our integrations that an object is typically scattered into the inner solar system the first time by a close encounter with Jupiter. In order for such an encounter to occur, the heliocentric distance of one of the object's node crossings must be at Jupiter's orbit. So, if we define r_a and r_d as the heliocentric distance of the ascending and descending nodes, respectively, a_J as Jupiter's semi-major axis, and $d_J = \min(|r_a - a_j|, |r_d - a_j|)$, then d_J should be close to zero just after an encounter with Jupiter (neglecting the small effect of Jupiter's eccentricity, which can lead to $d_J \lesssim 0.2\,AU$). Figure 9B shows the d_J distribution of the observed JFCs (bold curve) and simulated JFCs for three values of t_f. Just as with the inclinations, the distribution is best fit by $t_f \approx 10^4$ years.

It is possible to calculate a more accurate estimate of t_f by using Kolmogorov-Smirnov statistical test. In Figure 10, we plot as a dashed curve the probability that the inclination distribution derived from our integrations is the same as that observed as a function of t_f. The dotted curve is similar except for d_J. Note that both curves are very similar in shape and have a peak at the same place: $t_f = 12,000$ years. The curves show that we can rule out fade times of less than

~ 3000 years, or greater than $\sim 30,000$ years to a 90% confidence level. However, since there is no physical reason to expect that these two curves should agree to such an extent, the fact that the analysis of the inclination and d_j distributions agree to such a level adds credence to the idea that JFCs originate in the Kuiper belt and that the real value of t_f is about 10^4 years. We will adopt a value of $t_f = 12,000$ years in what follows.

We can extend this analysis to calculate the ratio of extinct to active visible ($q < 2.5\,AU$) JFCs in the solar system. The total number of visible JFCs in the solar system, N_{tot}, is the integral of $\xi(i)$ from Equation 1 over all inclinations. Similarly, the total number of active comets is the integral of $\xi_{active}(i)$. The number of extinct JFCs is thus $N_{tot} - N_{active}$. Figure 11 shows the relationship between the ratio of extinct to active JFCs as a function of t_f. Since we know that t_f lies between 3000 and 30,000 years, this ratio is between 2.0 and 6.7. If we assume $t_f = 12,000$ years then the ratio is 3.5.

With this information in hand, it is now possible to determine the total steady-state number of ecliptic comets that originated in the Kuiper belt, assuming all JFCs originated there. In the preceding calculations, we were interested in the population of comets with $q < 2.5\,AU$. Fernández et al. (1992) argued that the population of comets with total absolute magnitudes [2], H_T, brighter than 9 is complete for $q < 1.5\,AU$, but the population is not complete for $q > 1.5\,AU$. This incompleteness can be seen in Figure 12, which compares an estimate of the steady-state perihelion distribution of the population of known comets using data

[2] H_T is the total magnitude of an active comet. There is not necessarily a one-to-one relationship between H_T and the radius of a comet (which we would prefer to use). Unfortunately, there is no good estimate of the completeness of the JFCs as a function of radius.

presented by Fernández et al. (1992, solid curve) to that of our integration (dashed curve). In this figure, we scale the results from our integrations so that the total number of objects with $q < 1.5\,AU$ is the same in both curves. Figure 12 seems to indicate that the sample of observed comets is complete out to $q = 2\,AU$, but that there is significant observational incompleteness beyond $2\,AU$. From the data in Fernández et al. (1992), we estimate that the total number of objects with $H_T < 9$ and $q < 2\,AU$ is 40. From our integrations we find that about 37% of the visible comets have $q < 2\,AU$ (see Figure 12). Thus, there are approximately 108 active JFCs with $q < 2.5\,AU$ and $H_T < 9$ in the solar system.

The ratio of extinct to active comets of 3.5, as found above, implies that there are a total of ~ 500 JFCs with $q < 2.5\,AU$. We find from our integrations that at any instant the fraction of all our objects that are visible JFCs is 4.1×10^{-5}. Therefore, the current total number of ecliptic comets that correspond to objects with $H_T < 9$ and that originated in the Kuiper belt is 1.2×10^{7}. As noted in §3.4, $\sim 90\%$ of these objects are still beyond Neptune.

Using the above estimate, it is possible to project the results of our integration onto the sky and predict the number of objects observers should detect brighter than some limiting magnitude. In this estimate we assume that the observer is looking along the invariable plane, because we must correctly account for the variation of inclinations in our integration. In addition, we must also assume a size distribution and albedo for the bare nuclei of our comets. We adopt the size distribution that Weissman & Levison (1996) determined for the Kuiper belt of the form:

$$n(R)dn \propto \begin{cases} R^{-b_1}dR & \text{if } R \leq R_0 \\ R^{-b_2}dR & \text{if } R > R_0 \end{cases},$$

where $R_0 = 10\,km$, $b_1 = 3$, and $b_2 = 4.5$. In addition, we assume that there are no objects with $R > 200\,km$ and that the total of 1.2×10^{7} comets given above corresponds to objects $R > R_{min}$. As discussed above, since the relationship between H_T and radius is not well understood (if indeed such a relationship exists),

R_{min} is not well determined. We present our results for three values of R_{min}: $R_{min} = 0.5\,km$, $1\,km$, and $2\,km$. Clearly, the size distribution of these objects is still in considerable doubt (see Weissman & Levison 1996 for a discussion) and a complete survey of all the possible size distributions is beyond the scope of this paper. Therefore, we will adopt the above distribution as an illustrative case. We also assume an albedo of 0.04 and assume that no objects are discovered with heliocentric distances less than $10\,AU$, because their large drift rates against the background stars cause their images to be sufficiently trailed that they would not be discovered.

The results of projecting our model onto the sky are shown in Figure 13 in the form of the number of objects per square degree brighter than a visual magnitude V as a function of V. The three curves correspond to the three values of R_{min}. As a comparison, the results of various published searches for distant ecliptic comets have been included (see the figure caption for details). Of note are the searches by Kowal (1989: marked 'K' in the figure), which discovered Chiron, and by Jewitt et al. (1996: marked JLC), where two other Centaurs were discovered. For reasonable values of $2\,km > R_{min} \gtrsim 1\,km$, our model is in agreement with the results of both surveys and also predicts that none of the other published surveys should have detected ecliptic comets, which again is consistent. Jewitt et al. (1996) performed a simple analysis which suggested that they are discovering too many ecliptic comets in the searches. However, Figure 13 shows that this is not necessarily the case when a more accurate model such as ours is used. A more detailed comparison between our model and existing observations (such as those performed by Irwin et al. 1995 and Jedicke & Herron 1996) is left for a future paper.

We can use the total number of ecliptic comets calculated above to estimate the total number of objects in the same size range in the dynamically active region of the Kuiper belt between 30 and $50\,AU$. The rate at which objects leave the

Kuiper belt and become part of the ecliptic comet population must be balanced by the rate at which this population is removed from the solar system. Thus,

$$N_{KB}\ r_{Nx} = \frac{N_{EC}}{L_{EC}},$$

where N_{KB} and N_{EC} are the current numbers of comets in the Kuiper belt and ecliptic comet population, respectively, r_{Nx} is the fraction of particles that leave the Kuiper belt per year, and L_{EC} is the dynamical lifetime of an ecliptic comet. DLB95 estimate $r_{Nx} \approx 4 \times 10^{-11}$, although this assumption is based on an assumed orbital element distribution of objects in the Kuiper belt and thus is uncertain. From the previous paragraph, we find that $N_{EC} = 1.2 \times 10^{7}$. From §3.2, we find that $L_{EC} = 4.5 \times 10^{7}$ years. Therefore, $N_{KB} = 6.7 \times 10^{9}$ objects in the Kuiper belt within 50 AU. This number is consistent with our estimate of 5×10^{9} in DLB95.

5. Encounters with the Planets

In our integrations we kept track of the fraction of ecliptic comets that collide with the giant planets. With the above estimates of the total number of ecliptic comets, we can now estimate the impact rates on the giant planets. At one time such a calculation may have been thought to be irrelevant because an impact of a comet on a giant planet would have left no long-lived observational effect. However, with the spectacular impact of the comet D/1993F2 (Shoemaker-Levy 9) on Jupiter, the question of the impact rate of comets on the giant planets has become an important one. Our integrations may be of particular interest with regard to the D/1993F2 (Shoemaker-Levy 9) impact, since that comet was most likely a JFC (Dones et al. 1994; Chodas & Yeomans 1996; Benner & McKinnon 1995; Levison et al. 1996a).

As described in §3.2, approximately 1.5% of our objects experienced an impact with one of the giant planets. To be more precise, we find that the fractions of ecliptic comets that impact the planets are 0.0088, 0.0028, 0.0050, and 0.0045 for Jupiter through Neptune, respectively. In order to provide a steady-state population of ecliptic comets, the rate at which new ecliptic comets are injected from the Kuiper belt must be equal to $N_{EC}/L_{EC} \approx 0.27\,\mathrm{years}^{-1}$. The resultant impact rates for the giant planets are given in Table 1. Our results suggest that a JFC impact on Jupiter will happen once every 400 years. We probably witnessed such an event with the impact of D/1993F2 (Shoemaker-Levy 9) on Jupiter.

Although, as discussed above, we can calculate the impact rates of comets on the giant planets directly from our calculations, we have to estimate the impact rates on the terrestrial planets via other means, because they were not included in our integrations. We follow Öpik (1951), who calculated the probability that a comet will impact a planet as a function of both the comet's and the planet's orbital elements (also see Dones et al. 1996). The results of this calculation are also listed in Table 1. They suggest that an impact between a JFC and the Earth should happen once every 13 million years, which is the same as the more approximate estimate of Weissman (1995).

Several authors have attempted to estimate the impact rates of comets with planets. A complete discussion of this topic is beyond the scope of this paper (see Nakamura & Yoshikawa 1995 or Steel 1993 for a review). However, none of the earlier works had available to them an accurate representation of the distribution of comets in the outer solar system. In addition, most of these works used the Öpik equations (Öpik 1951), which are approximations, to calculate the impact rates. The few that used direct integrations, for example Nakamura & Yoshikawa (1995), used a very small number of comets and integrated for relatively short periods of time. As far as we know, the work presented here is the first to completely model the source of the impactors and the first to accurately count collisions with the outer planets.

Table 1

Impact Rates of Ecliptic Comets on the Planets

Planet	Rate comets/yr	Method of Calculation
Mercury	8.6×10^{-10}	Öpik
Venus	2.7×10^{-8}	Öpik
Earth	7.5×10^{-8}	Öpik
Mars	3.9×10^{-8}	Öpik
Jupiter	2.4×10^{-3}	Direct
Saturn	7.6×10^{-4}	Direct
Uranus	1.3×10^{-3}	Direct
Neptune	1.2×10^{-3}	Direct

In addition to impacts, it is possible that very close encounter with the giant planets might cause tidal disruption of comets and thus significantly alter the size distribution and the total number of the Jupiter family. D/1993F2 (Shoemaker-Levy 9) was disrupted due to a close encounter with Jupiter. In addition, comet 16P/Brooks2 was also believed to have been disrupted by a close encounter with Jupiter in 1886 (Sekanina & Yeomans 1985). In a recent work, Asphaug & Benz (1996) have shown that a comet will undergo breakup if its periapse at a planet is less than about 0.65 of the planet's classical Roche limit.

In Figure 14 we plot the fraction of comets that have a closest approach to a given planet at a distance r. Two sets of curves are shown. The solid curves are the results for our entire run, the dotted curves include only objects that became visible JFCs and include only encounters that happened before the comets first became visible. [3] The dashed line shows the location of the classical Roche limit. The figure shows that at most about 4% of all comets suffer a close enough encounter with a planet to disrupt it in its entire dynamical lifetime. Indeed, far less than 2Therefore, we conclude that the splitting or disruption of comets due to tidal encounters with the planets is not very important to the population of ecliptic comets as a whole.

[3] Note that this figure should not be interpreted as providing the distributions of encounter distances because each comet is included only once per planet at its closest encounter distance. However, in regions close to the planet where the probability of an encounter is small, the plotted distribution is probably close to the distribution of encounter distance.

6. Conclusions

In this paper we have presented numerical orbital integrations of 2200 massless particles as they evolved from Neptune-encountering orbits in the Kuiper belt, for a billion years or until they either impacted a massive body or were ejected from the solar system. The initial orbits for these particles were chosen from a previous set of integrations of objects that were initially in low-eccentricity, low-inclination orbits in the Kuiper belt but evolved onto Neptune-crossing orbits on timescales between 1 and 4 billion years (Duncan et al. 1995). We find that about 30% of these objects became visible comets. By visible we mean that, at least once, their perihelion distance q became less than $2.5\,AU$. Of those that became visible, 99.7% were Jupiter-family comets at the time of first visibility.

Thus, we now have a complete model of the origin of the Jupiter-family comets. In this model we show that objects in the Kuiper belt can remain in low- to moderate-eccentricity orbits for timescales comparable to the age of the solar system and then evolve onto Neptune-encountering orbits (Duncan et al. 1995). The primary mechanism for this instability is the overlap of resonances, both mean motion and secular, with the giant planets. Here we have shown that these objects evolve into a population of visible comets that are dynamically indistinguishable from the observed Jupiter family. Working backwards from the observed number of Jupiter-family comets, we find a physically reasonable population of comets ($\sim 7 \times 10^9$) in the Kuiper belt, consistent with earlier estimates (Duncan et al. 1998), mass limits (Yeomans 1986; Hamid et al. 1968) and the recent Hubble Space Telescope observations (Cochran et al. 1995).

We have used the integrations presented here to study the distribution and fates of objects which have left the Kuiper belt at the current epoch. We have reached the following conclusions about this distribution:

1. As objects evolve inward from the Kuiper belt, they tend to be under the dynamical control of one planet. That planet will scatter the comets inward and outward in a random walk, typically handing them off to the planet directly interior or exterior to it. Therefore, the comets tend to have eccentricities of about 25% between handoffs. However, once they have been scattered into the inner solar system by Jupiter, they can have much larger eccentricities as they evolve outward.

2. The very narrow range in the Tisserand parameter, T, with respect to Jupiter of the JFCs is mainly due to the fact that when they were on their initial Neptune-encountering orbits, the comets had a narrow range in the Tisserand parameter with respect to Neptune.

3. The median dynamical lifetime of the ecliptic comets is 4.5×10^7 years. This is the time from the first encounter with Neptune to ejection from the solar system, placement in the Oort cloud, or impact with the Sun or a planet.

4. About 5% of the particles survived the length of the integration (10^9 years). All of the survivors had semi-major axes outside the orbit of Neptune. This implies that there may be a significant population of objects with highly eccentric orbits in an extended disk beyond the orbit of Neptune. This 'scattered' Kuiper belt may be particularly massive if the primordial Kuiper belt was more massive than it is today (see Stern 1995 or Levison et al. 1996b for a discussion of this).

5. Although when the ecliptic comets first become visible they are almost entirely members of the Jupiter family, a small fraction of these comets switch to visible Halley-type comets. Since those that switch have longer dynamical lifetimes, on average about 13% of all visible ($q < 2.5\,AU$) comets derived from the Kuiper belt with $a < 40\,AU$ will be HTCs. However, the orbital element distribution

of the simulated HTCs is not consistent with the observed distribution. Since we find that it takes at least 10^5 years and usually over 10^6 years to become a visible HTC after the comet first becomes visible, we conclude that most of these comets have likely become extinct. Thus, although the Kuiper belt can be the source of at least some of the HTC, it cannot provide a significant number of them.

6. By comparing the orbital element distribution of our simulated JFCs to that of observed JFCs, we estimate the physical lifetime of JFCs is between 3000 and $30,000$ years. The most likely value is $12,000$ years. From this we estimate that the ratio of extinct to active JFCs is 3.5 and that the total number of ecliptic comets is 1.2×10^7. The latter estimate refers to objects that produce comets with total absolute magnitudes brighter than 9. Since the relationship between total absolute magnitudes and radius is not well understood and a comet will become fainter as it ages, this number should be viewed as an effective lower limit.

7. We have directly measured the impact rates with the giant planets in our simulations. In addition, we have estimated the impact rates with the terrestrial planets using Öpik's equations. These rates are given in Table 1. We find that an ecliptic comet will impact Jupiter once every 400 years. The impact interval on the Earth is estimated to be 13 Myr.

We would like to thank L. Dones, C. Chapman, A. Stern, S. Tremaine, G. Stewart, and P. Weissman for helpful discussions. We are also grateful to J. Fernández and M. Holman for providing insightful comments as the referees of this manuscript. HFL gratefully acknowledges grants provided by the NASA Origins of Solar Systems and Planetary Geology and Geophysics Programs. MJD is grateful for the continuing financial support of the Natural Science and Engineering Research

Council of Canada and for financial support for work done in the U.S. from NASA Planetary Geology and Geophysics Programs. We also gratefully acknowledge funding for our computer equipment from the National Science Foundation and the Southwest Research Institute.

REFERENCES

A'Hearn, M.F., Millis, R.L., Schleicher, D.G., Osip, D.J., & Birch, P.V. 1995. 'The ensemble properties of comets : results from narrow-band photometry of 85 comets, 1976-1992.' *Icarus* **118**, 223-270.

Asher, D.J., & Steel, D.I. 1993. 'Orbital evolution of the large outer solar system object 5145 Pholus.' *Mon. Not. Roy. Astron. Soc.* **263**, 179-190.

Asphaug, E., & Benz, W. 1996. 'Size, density and structure of comet Shoemaker-Levy 9 inferred from the physics of tidal breakup.' *Icarus* **121**, 225-248.

Benner, L.A.M. & McKinnon, W. 1995. 'On the orbital evolution and origin of comet Shoemaker-Levy 9.' *Icarus* **118**, 155-168.

Carusi A., & Valsecchi, G. 1987, 'Dynamical Evolution of Short-Period Comets' in *Interplanetary Matter*, eds. Z. Ceplecha & P. Pecina (Ondrejov: Czechoslovak Academy of Sciences), 21-28.

Chodas, P.W. & Yeomans, D.K. 1996. In *The Collision of Comet Shoemaker-Levy 9 and Jupiter*, eds. K. Noll, P.D. Feldman, & H.A. Weaver (Cambridge: Cambridge University Press), 1.

Cochran, A.L., Cochran, W.D. & Torbett, M.V. 1991. 'A deep imaging search for the Kuiper disk of comets.' *Bull. AAS* **23**, 1314.

Cochran, A., Levison, H., Stern, S.A., & Duncan, M. 1995. 'The discovery of Halley-sized Kuiper belt objects using the Hubble Space Telescope.' *Astrophys. J.* **455**, 342-346.

Dones, L., Levison, H., & Duncan, M. 1994. 'Possible orbital histories of comet Shoemaker-Levy 9.' *Bull. AAS* **26**, 861.

Dones, L., Levison, H., & Duncan, M. 1996. 'On the dynamical lifetimes of planet-crossing orbits.' To appear in *Completing the Inventory of the Solar System*, ed. T.W. Rettig.

Duncan, M., Quinn, T., & Tremaine, S. 1987. 'The formation and extent of the solar system comet cloud.' *Astron. J.* **94**, 1330-1338.

Duncan, M., Quinn, T., & Tremaine, S. 1988. 'The origin of short-period comets.' *Astrophys. J. Letters* **328**, L69-L73.

Duncan, M., Levison, H., & Budd, M. 1995. 'The dynamical structure of the Kuiper belt.' *Astron. J.* **110**, 3073-3081.

Everhart, E. 1977. 'The evolution of comet orbits as perturbed by Uranus and Neptune.' In *Comets–Asteroids–Meteorites,* ed. A.H. Delsemme (Ohio: University of Toledo Press), 99-104.

Fernández, J. 1980. 'On the existence of a comet belt beyond Neptune.' *Mon. Not. Roy. Astron. Soc.* **192**, 481-491.

Fernández, J., & Ip., W.-H. 1984. 'Some dynamical aspects of the accretion of Uranus and Neptune - the exchange of orbital angular momentum with planetesimals.' *Icarus* **58**, 109-120.

Fernández, J.,& Ip W.-H. 1991. 'Statistical and evolutionary aspects of cometary orbits.' In *Comets in the Post-Halley Era: IAU Coll. 116*, eds. R. L. Newburn, J. Rahe & M. Neugebauer (Amsterdam: Kluwer), 487-535.

Fernández, J., Rickman, H. & Kamel, L. 1992. 'The population size and distribution of perihelion distances of the Jupiter family.' In *Proceedings of the International Workshop on Periodic Comets*, eds. J. Fernández and H. Rickman (Montevideo: Universidad de la Republica Publicaciones), 143-158.

Gladman, B., & Duncan, M. J. 1990. 'On the fates of minor bodies in the outer solar system.' *Astron. J.* **100**, 1680-1693.

Hahn, G. & Bailey, M.E. 1990. 'Rapid dynamical evolution of giant comet Chiron.'

Nature **348**, 132-136.

Hamid, S.E., Marsden, B.J., & Whipple, F.L. 1968. 'Influence of a comet belt beyond Neptune on the motions of periodic comets.' *Astron. J.* **73**, 727-729.

Holman, M., & Wisdom, J. 1993. 'Dynamical stability of the outer solar system and the delivery of short-period comets.' *Astron. J.* **105**, 1987-1999.

Irwin, M., Tremaine, S., & Zytkow, A.N. 1995. 'A search for slow-moving objects and the luminosity function of the Kuiper belt.' *Astron. J.* **110**, 3082-3093.

Jedicke, R., & Herron, J.D. 1996. 'An observational limit on the number of Centaur asteroids.' Submitted to *Icarus*.

Jewitt, D., & Luu, J. 1995. 'The solar system beyond Neptune.' *Astron. J.* **109**, 1867-1876.

Jewitt, D., Luu, J., Chen, J. 1996. 'The Mauna Kea - Cerro Tololo (MCKT) Kuiper belt and Centaur Survey.' *Astron. J.* **112**, 1225-1238.

Kazimirchak-Polonskaya, E. I. 1972. 'The major planets as powerful transformers of cometary orbits.' In *The Motion, Evolution of Orbits, and Origin of Comets: IAU Symposium 45*, eds. G.A. Chebotarev, E.I. Kazimirchak-Polonskaya, & B.G. Marsden. (Dordrecht: Reidel), 156-166.

Kowal, C. 1989. 'A solar system survey.' *Icarus* **77**, 118-123.

Levison, H. 1996. 'Comet taxonomy.' To appear in *Completing the Inventory of the Solar System*, ed. T.W. Rettig.

Levison, H., & Duncan, M. 1990. 'A search for proto-comets in the outer regions of the solar system.' *Astron. J.* **100**, 1669-1675.

Levison, H., & Duncan, M. 1993. 'The gravitational sculpting of the Kuiper belt.' *Astrophys. J. Lett.* **406**, L35-L38.

Levison, H., & Duncan, M. 1994. 'The long-term behaviour of short-period comets.' *Icarus* **108**, 18-36.

Levison, H., Shoemaker, E.M., & Shoemaker, C.S. 1996a. 'The dispersal of the

Trojan asteroid swarm.' Submitted to *Nature.*

Levison, H., Stern, S.A. & Duncan, M. 1996b. 'The role of a massive primordial Kuiper belt on its current structure.' In preparation.

Luu, J., & Jewitt, D. 1988. 'A two-part search for slow-moving objects.' *Astron. J.* **95**, 1256-1262.

Nakamura, T., & Yoshikawa, M. 1995. 'Close encounters and collisions of short-period comets with Jupiter and its satellites.' *Icarus* **116**, 113-124.

Oikawa, S., & Everhart, E. 1979. 'Past and future orbit of 1977 UB, object Chiron.' *Astron. J.* **84**, 134-139.

Öpik, E.J. 1951. 'Collision probabilities with the planets and the distribution of interplanetary matter.' *Proc. Roy. Irish Acad.* **54A**, 165-199.

Quinn, T.R., Tremaine, S., & Duncan, M.J. 1990. 'Planetary perturbations and the origin of short period comets.' *Astrophys. J.* **355**, 667-679.

Scholl, H. 1979. 'History and evolution of Chiron's orbit.' *Icarus* **40**, 345-349.

Sekanina, Z., & Yeomans, D.K. 1985. 'Orbital motion, nucleus precession and splitting of periodic comet Brooks 2.' *Astron. J.*, **90**, 2335-2352.

Steel, D.I. 1993. 'Collisions in the solar system. V. Terrestrial impact probabilities for parabolic orbits.' *Mon. Not. R. Astron. Soc.* **264**, 813-817.

Stern, S.A. 1995. 'Collision timescales in the Kuiper disk and their implications.' *Astron. J.* **110**, 856-867.

Torbett, M. 1989. 'Chaotic motion in a comet disk beyond Neptune - the delivery of short-period comets.' *Astron. J.* **98**, 1477-1481.

Weissman, P. 1995. In *Hazards Due to Comets and Asteroids,* ed. T. Gehrels (Tucson: University of Arizona Press), 1191.

Weissman, P., & Levison, H. 1996. 'The population of the trans-Neptunian region: the Pluto-Charon environment.' To appear in *Pluto*, eds. D.J. Tholen and S.A. Stern.

Wetherill, G.W. 1991. 'End-products of cometary evolution : cometary origin of Earth-crossing bodies of asteroidal appearance.' In *Comets in the Post-Halley Era: I.A.U. Coll. 116*, eds. R. L. Newburn, J. Rahe & M. Neugebauer (Amsterdam: Kluwer), 537-556.

Wisdom, J., & Holman, M. 1991. 'Symplectic maps for the n-body problem.' *Astron. J.* **102**, 1528-1538.

Yabushita, S. 1980. 'On exact solutions of diffusion equations in cometary dynamics.' *Astron. & Astrophy.* **85**, 77-79.

Yeomans, D.K. 1986. 'Physical interpretations from the motions of comets Halley and Jacobini-Zinner.' In *Twentieth ESLAB Symposium on the Exploration of Halley's Comet Vol. II*, eds. B. Battrick, E.J. Rolfe & R. Reinhard, ESA SP-250. (Nordrick : European Space Agency), 419-425.

Figure Captions

Figure 1 — The inclinations of objects leaving the Kuiper belt after being stable for at least 1 billion years as a function of their initial semi-major axes. All these particles had initial $i = 1°$. Different symbols refer to the initial eccentricities of the particles. These data were taken from Duncan et al. (1995, cf. their Figure 7). The important mean motion resonances are also shown. Objects used as initial conditions for the integrations reported in this paper are highlighted by gray dots.

Figure 2 — A) The semi-major axes, a, of observed comets with periods less than 200 years as a function of their Tisserand parameter with respect to Jupiter, T. The dashed vertical lines represent the boundaries of the Jupiter family at $T = 2$ and $T = 3$. Objects falling above the solid curve must have perihelia greater than $2.5\,AU$. B) The inclination, i, of the same set of comets as in Figure 2A as a function of T. Again, the dashed lines represent the boundaries of the Jupiter family. The shaded areas represent regions that are physically unattainable due to the relationship between i and T assuming $q \leq 2.5\,AU$ and $Q \geq a_J$. C) The same as Figure 2A except for our simulated comets when they first become visible, i.e., when their perihelia first drop below $2.5\,AU$. D) The same as Figure 2B except for simulated comets when they first become visible.

Figure 3 — The evolution of a representative particle originating in the Kuiper belt. A) The Tisserand parameter of this particle with respect to each giant planet as a function of time. Different colors represent different planets: blue is Jupiter, red is Saturn, green is Uranus, and black is Neptune. The circles and dashes indicate if the test particle is planet-crossing or not, respectively.

B) Locations of the particle's orbit in the q–Q (perihelion-aphelion) plane are joined by blue lines until the particle became 'visible' ($q < 2.5$ AU) and are linked in red thereafter. The sampling interval was every 10^4 years in the previsibility phase and every 10^3 years thereafter. Also shown in the figure are three lines of constant eccentricity at $e = 0$, 0.2, and 0.3. In addition, we plot two dashed curves of constant semi-major axis, one at Jupiter's orbit and one at its 2:1 mean motion resonances.

Figure 4 — The relationship between inclinations of comets and their perihelia as they evolve inward from the Kuiper belt. This histogram does not include objects after they have become visible comets. The inclination is represented as the mean of the cosines of the inclination. The locations of the four giant planets are also shown for reference.

Figure 5 — Relationships between the orbital elements of visible comets and their initial orbits. Here, we refer to the orbit that an object had as it left the Kuiper belt as the 'initial orbit.' A) The fraction of comets that become visible JFCs as a function of their initial Tisserand parameter with respect to Neptune. B) The mean cosine of inclinations of comets when they first become visible as a function of their initial orbits. C) The mean Tisserand parameter with respect to Jupiter, T, of comets when they first become visible as a function of their initial Tisserand parameter with respect to Neptune. See text for a discussion of how our particles were grouped to form the means.

Figure 6 — A contour plot of the relative distribution of ecliptic comets in the solar system as a function of aphelion (Q) and perihelion (q). The units are the fraction of comets per square AU in q–Q. Also shown in the figure are three lines of constant eccentricity at $e = 0$, 0.2, and 0.3. In addition, we plot two dashed curves of constant semi-major axis, one at Jupiter's orbit and one at

its 2:1 mean motion resonance. They gray dot labeled 'E' shows the location of comet 2P/Encke. The label '1:2' indicates the location of Neptune's 1:2 mean motion resonance.

Figure 7 — The temporal behavior of a particle that evolves onto a nearly circular orbit in Neptune's 1:2 mean motion resonance. The solid curve and dotted curve, respectively, show the particle's semi-major axis, a, and perihelion distance, q, as a function of time. At $t = 1.54 \times 10^9$ years, this particle has $e = 0.0003$. Also shown in this figure are the locations of Neptune's orbit and several of its mean motion resonances.

Figure 8 — The surface density of ecliptic comets in the solar system as a function of heliocentric distance. The curve is normalized so that the total number of comets is one. Therefore, the units of the plot are the fraction of comets per square AU.

Figure 9 — A) The integrated inclination distribution of visible Jupiter-family comets. The bold solid curve is the observed distribution. The three dotted curves shows the distribution for simulated comets for different values of the fade time, t_f. B) Same as Figure 9A except we plot the d_J distribution. See text for the definitions of t_f and d_J.

Figure 10 — The dashed curve shows the probability that the inclination distribution of visible Jupiter-family comets produced in our simulation is the same as that observed in nature as a function of the fade time t_f. The comparison was made by using a Kolmogorov-Smirnov (K-S) test. The dotted curve is the same but for the d_J distribution. See text for the definitions of t_f and d_J. Both curves have a peak at $12,000$ years.

Figure 11 — The ratio of the number of extinct to active visible ($q < 2.5\,AU$) Jupiter-family comets as a function of the fade time, t_f, as predicted by our simulations.

Figure 12 — The solid curve represents the average perihelion distance distribution of the known active JFCs with $H_T < 9$ as determined from data in Fernández et al. (1992). The error bars represent 1σ statistical Poisson errors. The dashed curve is the steady state perihelion distribution of our model. We scale the results from our integrations so that the total number of objects with $q < 1.5\,AU$ is the same as that observed.

Figure 13 — The curves in this figure show the predicted number of ecliptic comets per square degree of sky along the ecliptic from our model. The three curves represent three values of R_{min}: $0.5\,km$, $1\,km$, and $2\,km$. As a comparison, we plot the results of several published searches (upper limits are shown for searches that did not find any ecliptic comets) as a function of limiting magnitude. Photographic surveys have been performed by Luu & Jewitt (1988: LJ88(S)), in which they covered $200\,\mathrm{deg}^2$ to a V limit of 20 with a Schmidt telescope and plates, and by Kowal (1989: K), reaching a limiting V magnitude of 20 for $6400\,\mathrm{deg}^2$. Kowal discovered Chiron in his survey. CCD surveys include Luu & Jewitt (1988: LJ88(CCD)), which covered $0.34\,\mathrm{deg}^2$ to a V limit of 24.5. Levison & Duncan (1990: LD) performed the largest CCD survey, covering $4.9\,\mathrm{deg}^2$ to a V magnitude of 22.5. The survey of Cochran et al. (1991: CCT) was a CCD survey in V and R which had reached a limiting magnitude of 24 in V, and covered $\sim 0.75\,\mathrm{deg}^2$. Jewitt & Luu (1995: LJ95) performed a CCD search that had a limiting magnitude of 25 and a coverage of $1\,\mathrm{deg}^2$. They discovered several Kuiper belt objects with this survey, but no ecliptic comets. Most recently, Jewitt et al. (1996: JLC) surveyed $3.9\,\mathrm{deg}^2$

to a limiting R magnitude of 24.2 and found two Centaurs, implying a density of 0.5 ± 0.4 objects per square degree.

Figure 14 — The distribution of close approaches between comets in our simulation and the giant planets. Note that this figure should not be interpreted as the distributions of encounter distances, because each comet is included only once per planet at its closest encounter distance. The solid curves shows the results for our entire run. The dotted curves include only objects that became visible JFCs. In addition, for the dotted curves we include only encounters that occurred before the comet became visible. The dashed lines show the locations of the classical Roche limits of the respective planets.

FIGURE 1

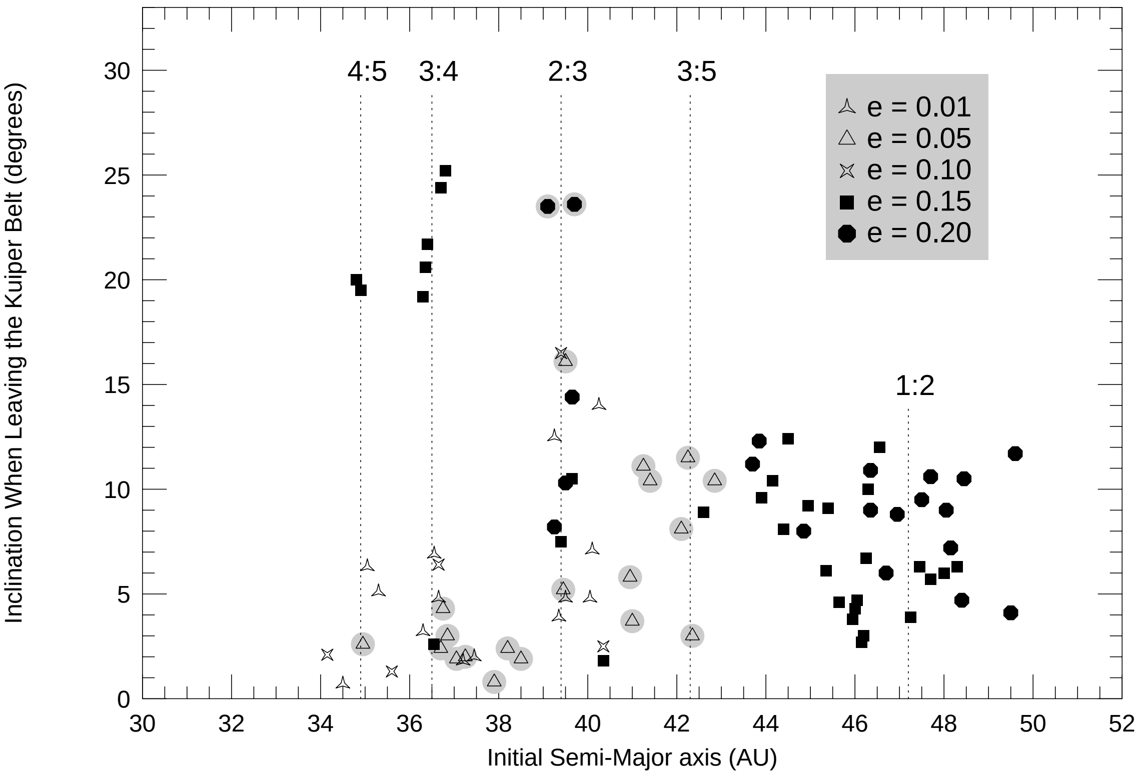

4:5
3:4
2:3
3:5
1:2
e = 0.01
e = 0.05
e = 0.10
e = 0.15
e = 0.20
Inclination When Leaving the Kuiper Belt (degrees)
Initial Semi-Major axis (AU)

FIGURE 2

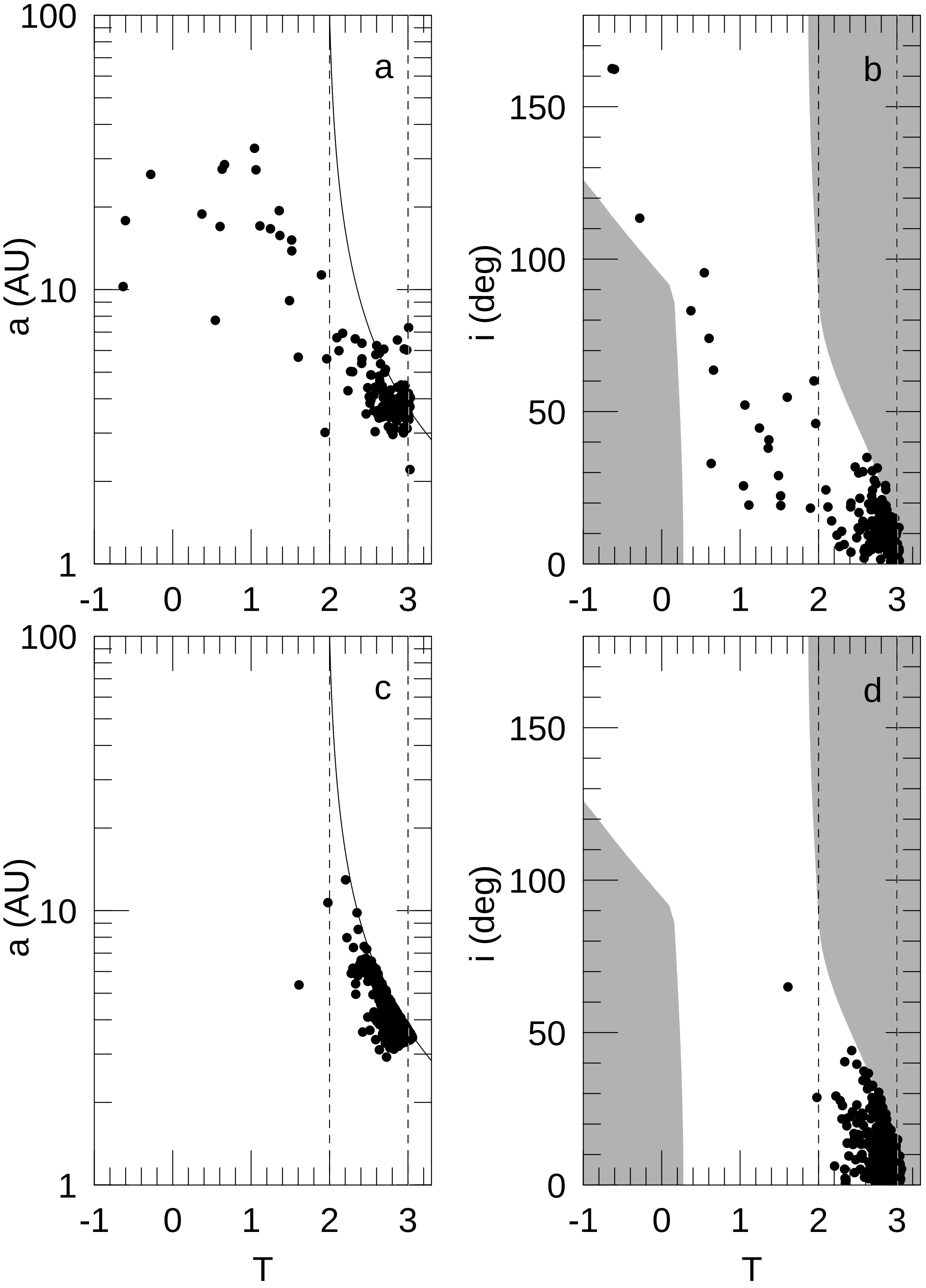

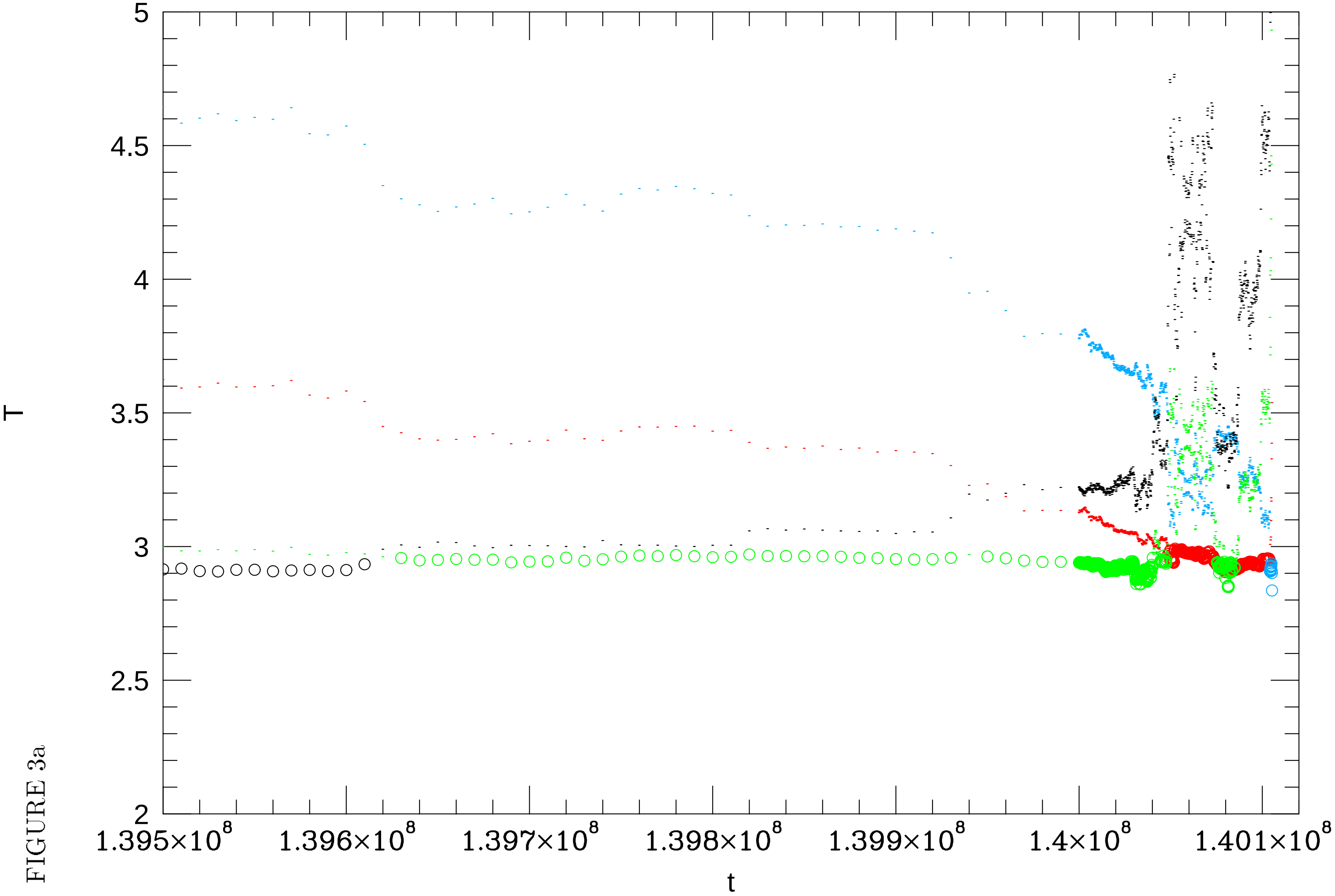
T
5
4.5
4
3.5
3
2.5
2
1.395×10^8
1.396×10^8
1.397×10^8
1.398×10^8
1.399×10^8
1.4×10^8
1.401×10^8
t

FIGURE 3a

FIGURE 3b

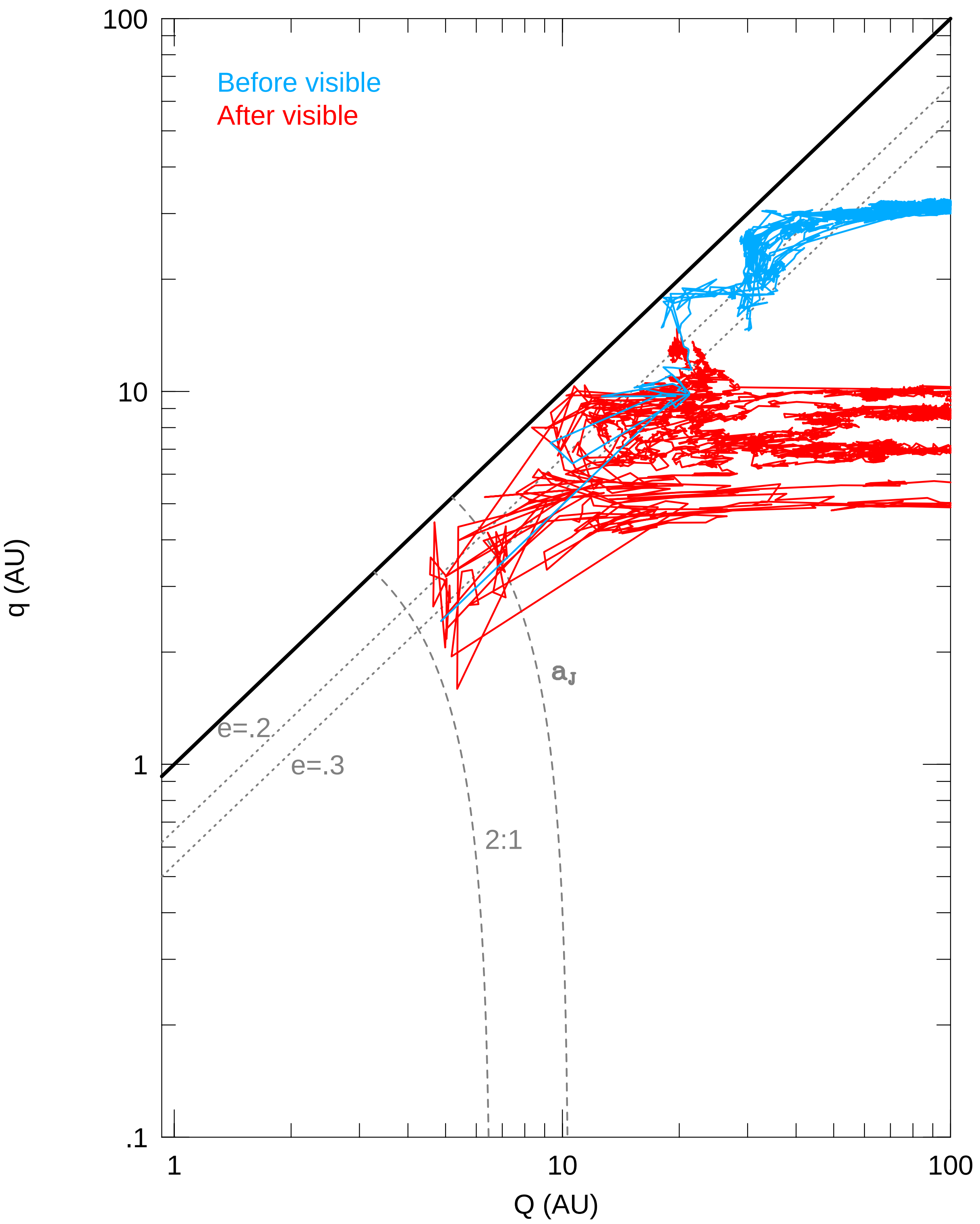

Before visible
After visible
100
10
1
.1
q (AU)
1
10
100
Q (AU)
e=.2
e=.3
2:1
a_J

FIGURE 4

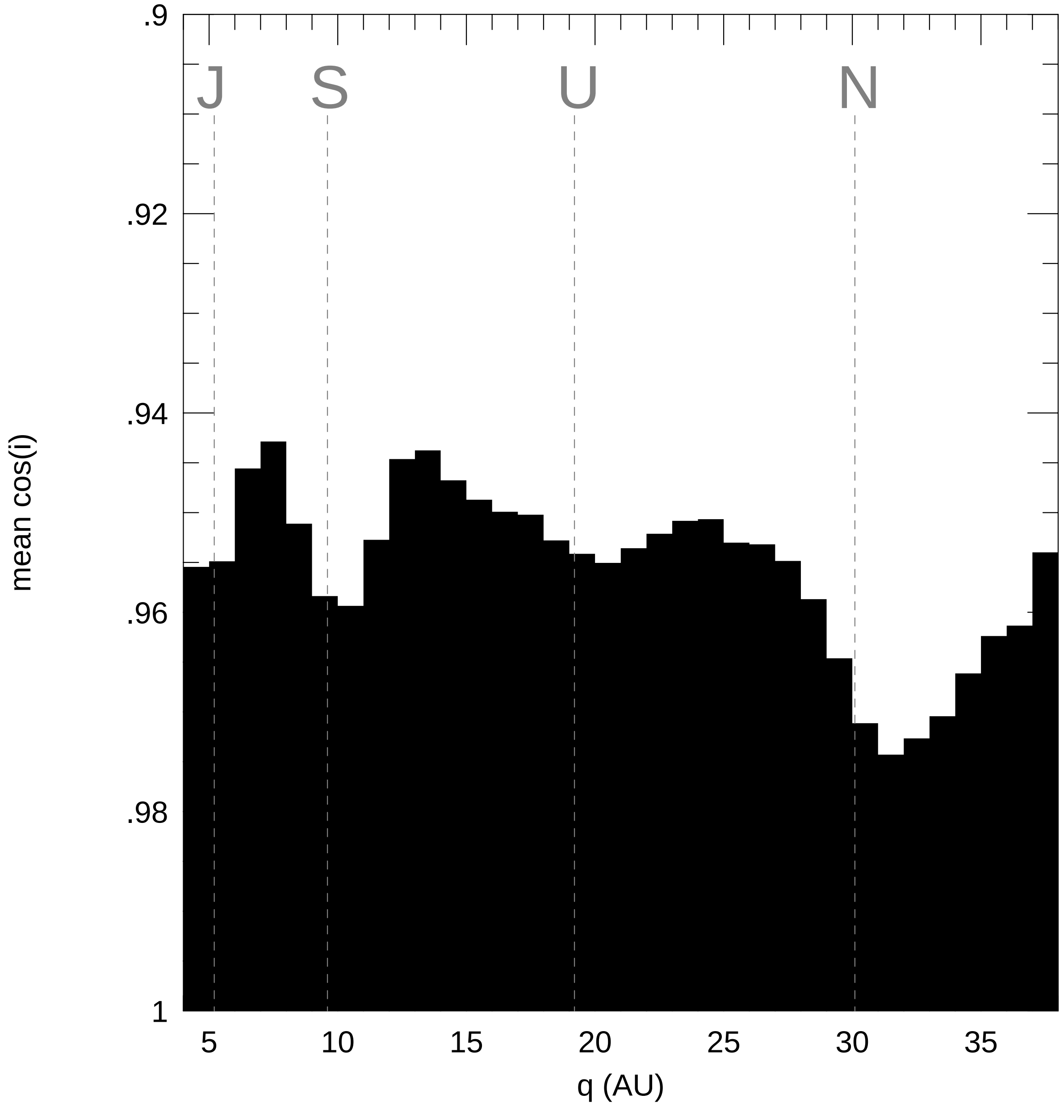

FIGURE 5

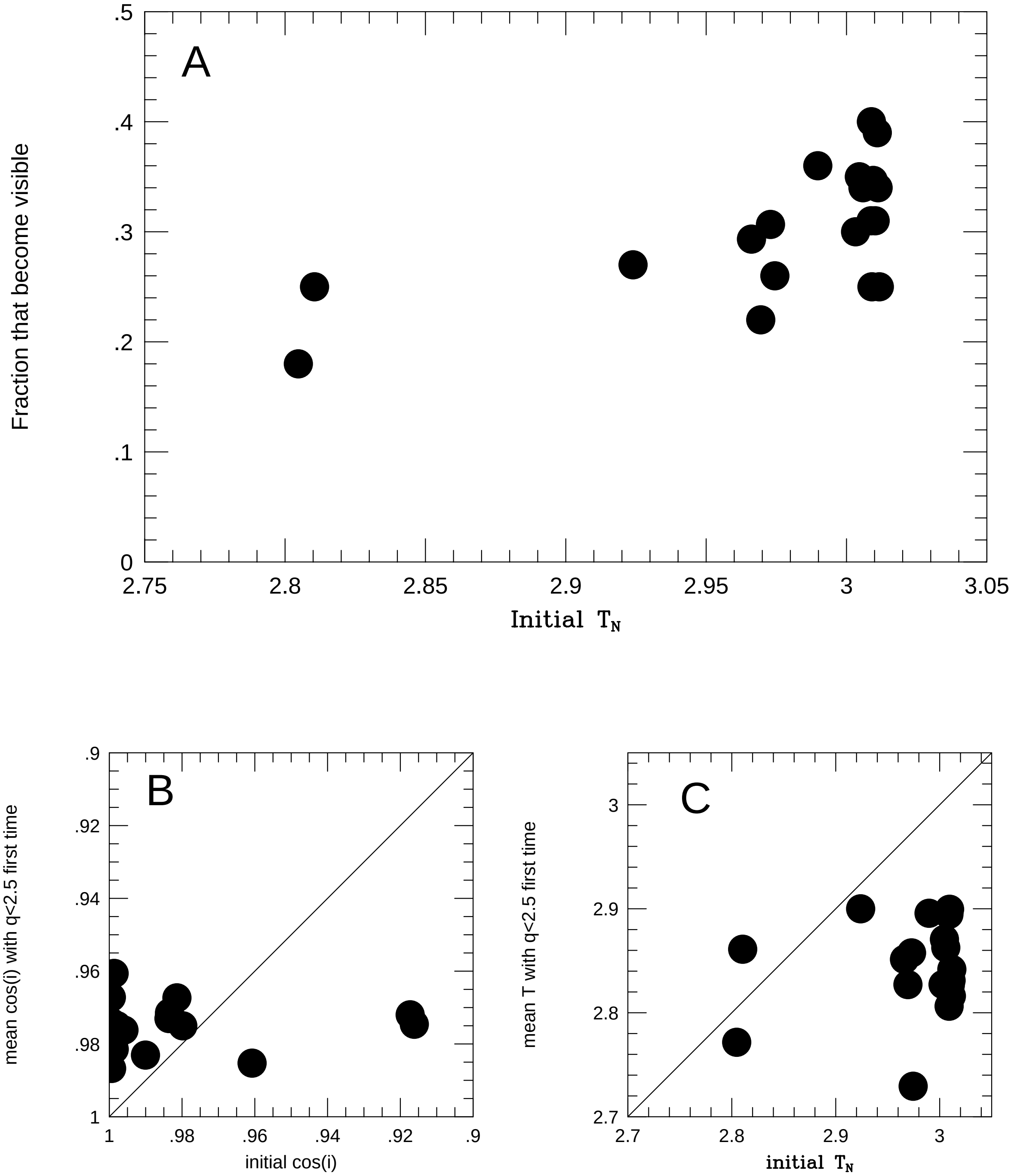

A
Fraction that become visible
Initial T_N
B
mean cos(i) with q<2.5 first time
initial cos(i)
C
mean T with q<2.5 first time
initial T_N

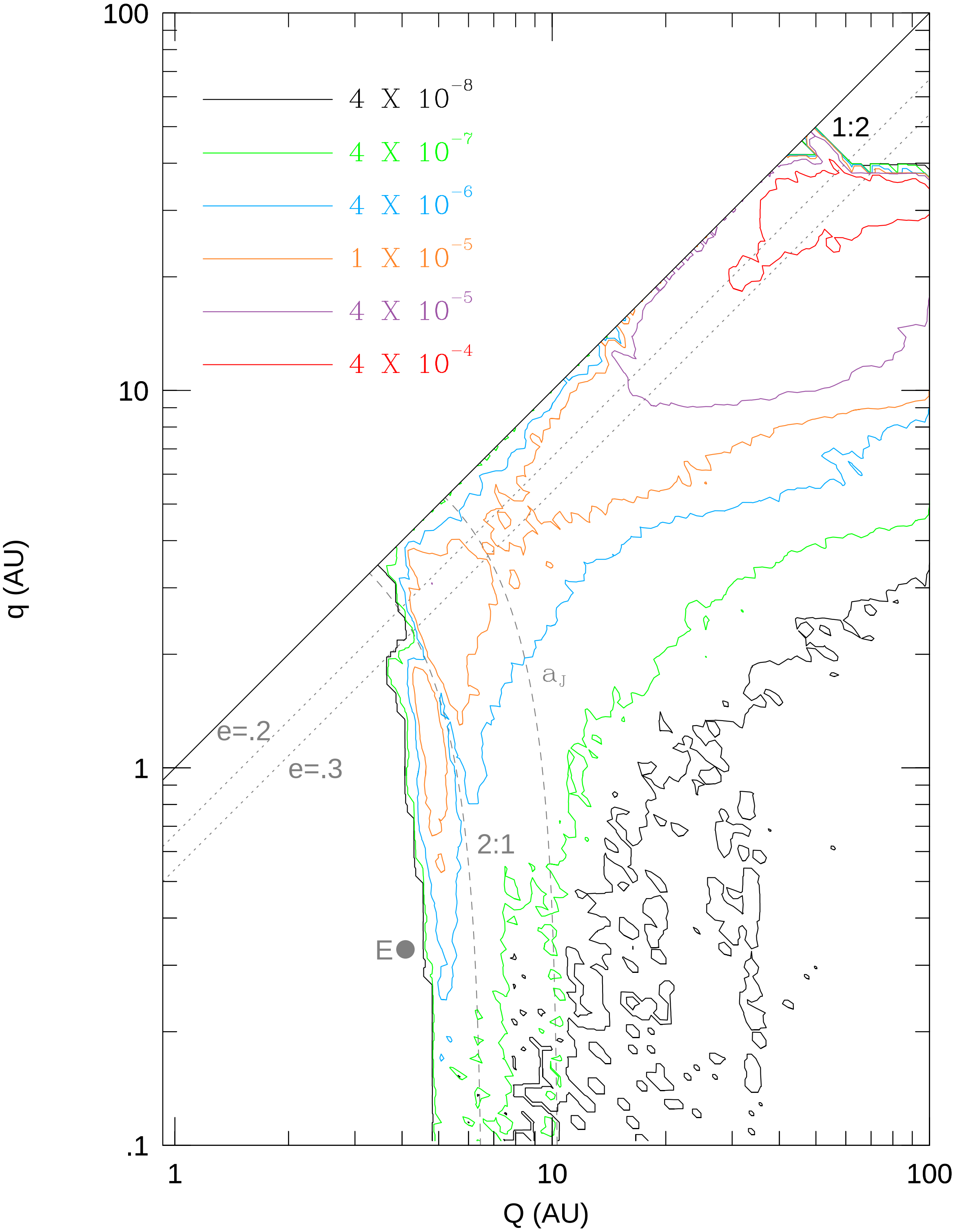

4 X 10^{-8}
4 X 10^{-7}
4 X 10^{-6}
1 X 10^{-5}
4 X 10^{-5}
4 X 10^{-4}
1:2
e=.2
e=.3
a_J
2:1
E
100
10
1
.1
q (AU)
Q (AU)

FIGURE 6

FIGURE 7

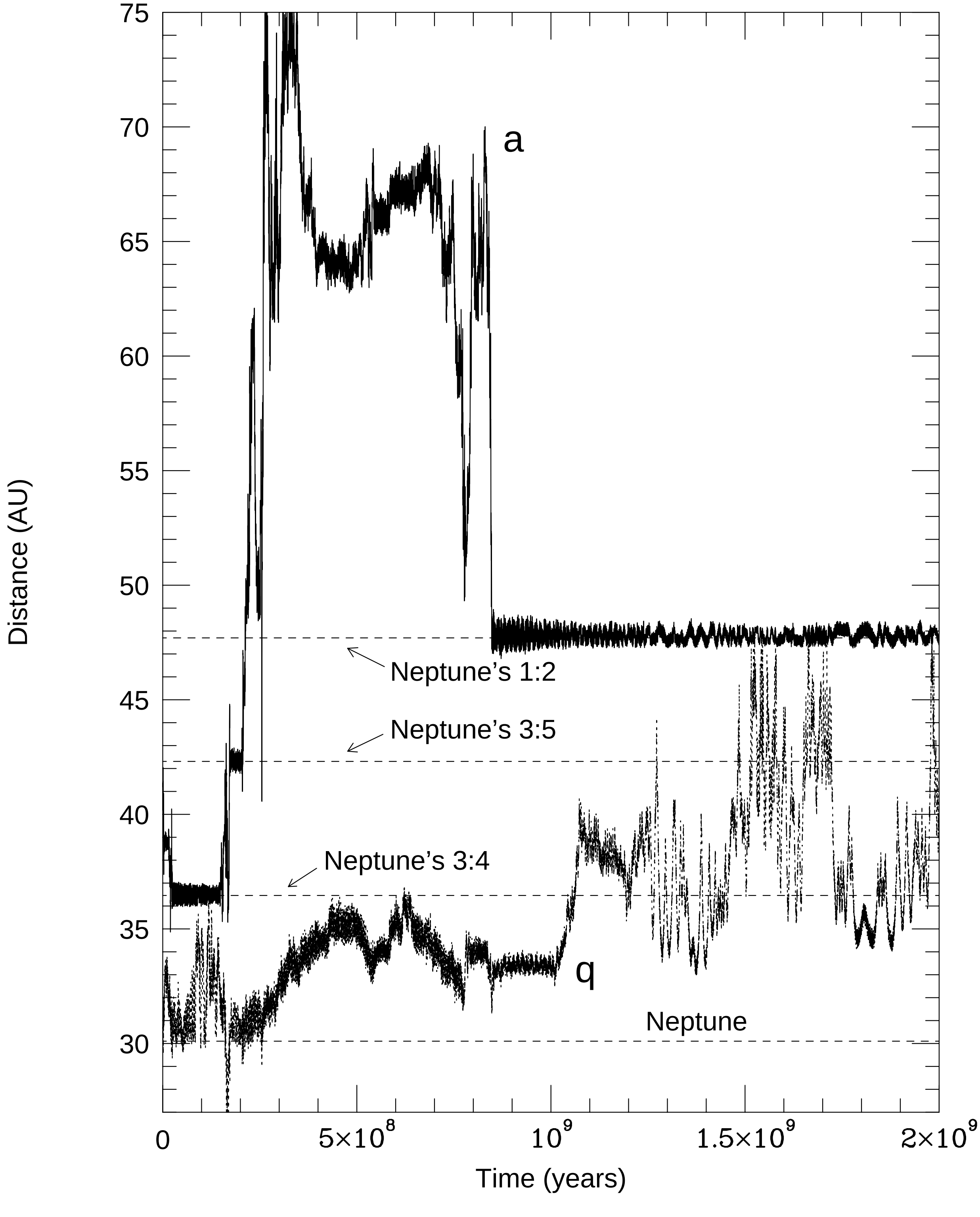

75
70
65
60
55
50
45
40
35
30
Distance (AU)
a
q
Neptune's 1:2
Neptune's 3:5
Neptune's 3:4
Neptune
0
5×10^8
10^9
1.5×10^9
2×10^9
Time (years)

FIGURE 8

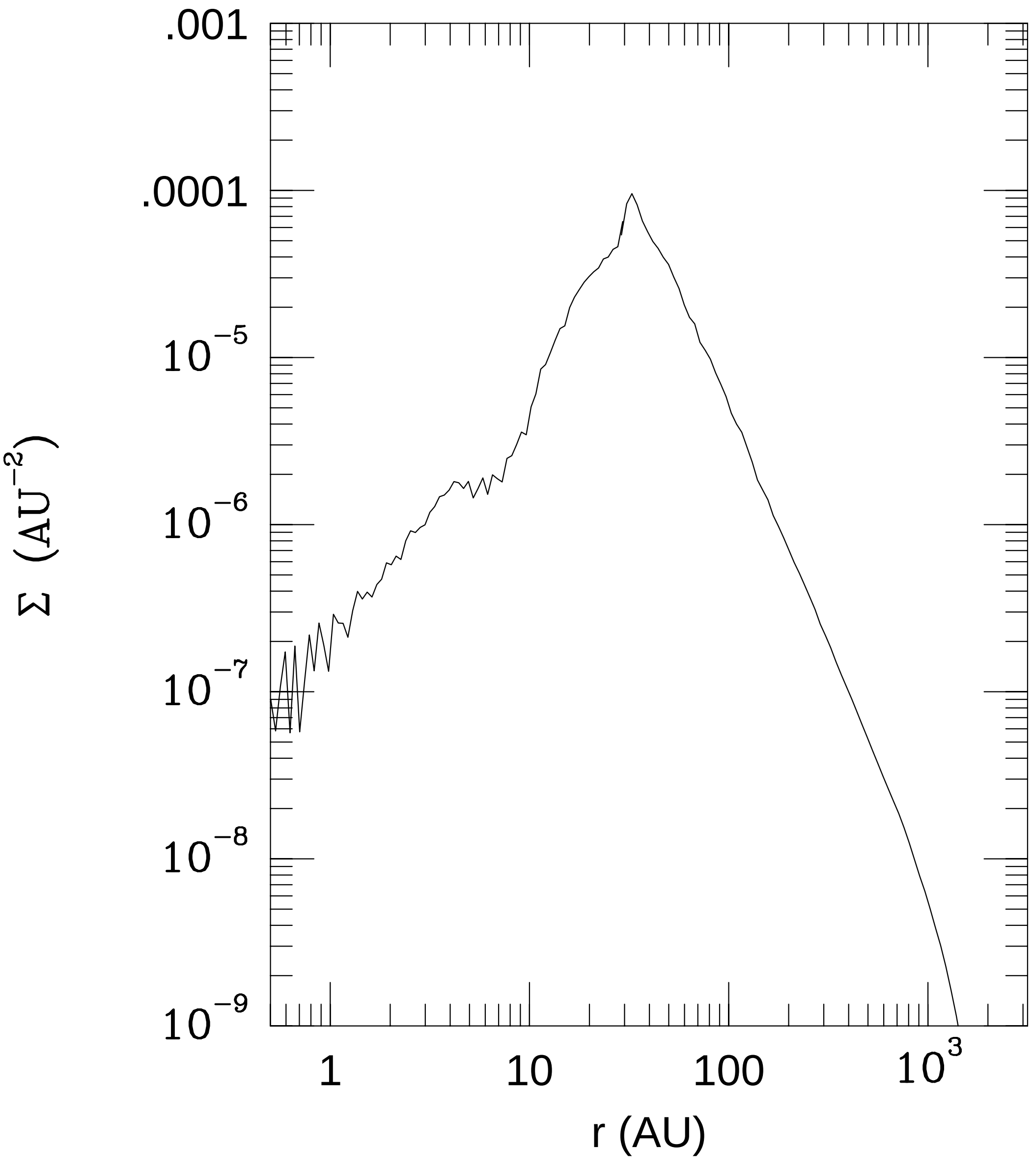

FIGURE 9

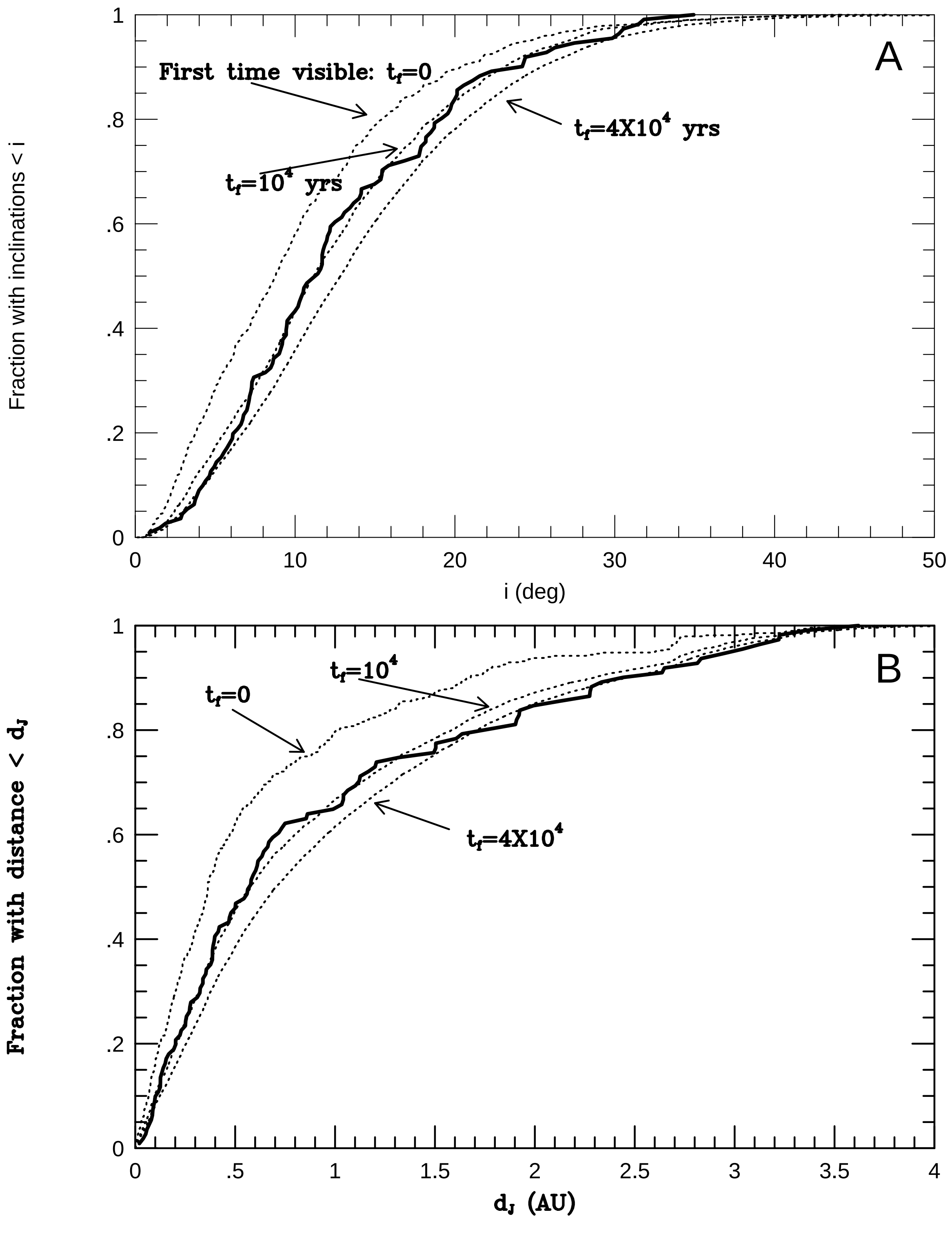

A
First time visible: t_f=0
t_f=10^4 yrs
t_f=4X10^4 yrs
Fraction with inclinations < i
i (deg)
B
t_f=0
t_f=10^4
t_f=4X10^4
Fraction with distance < d_J
d_J (AU)

FIGURE 10

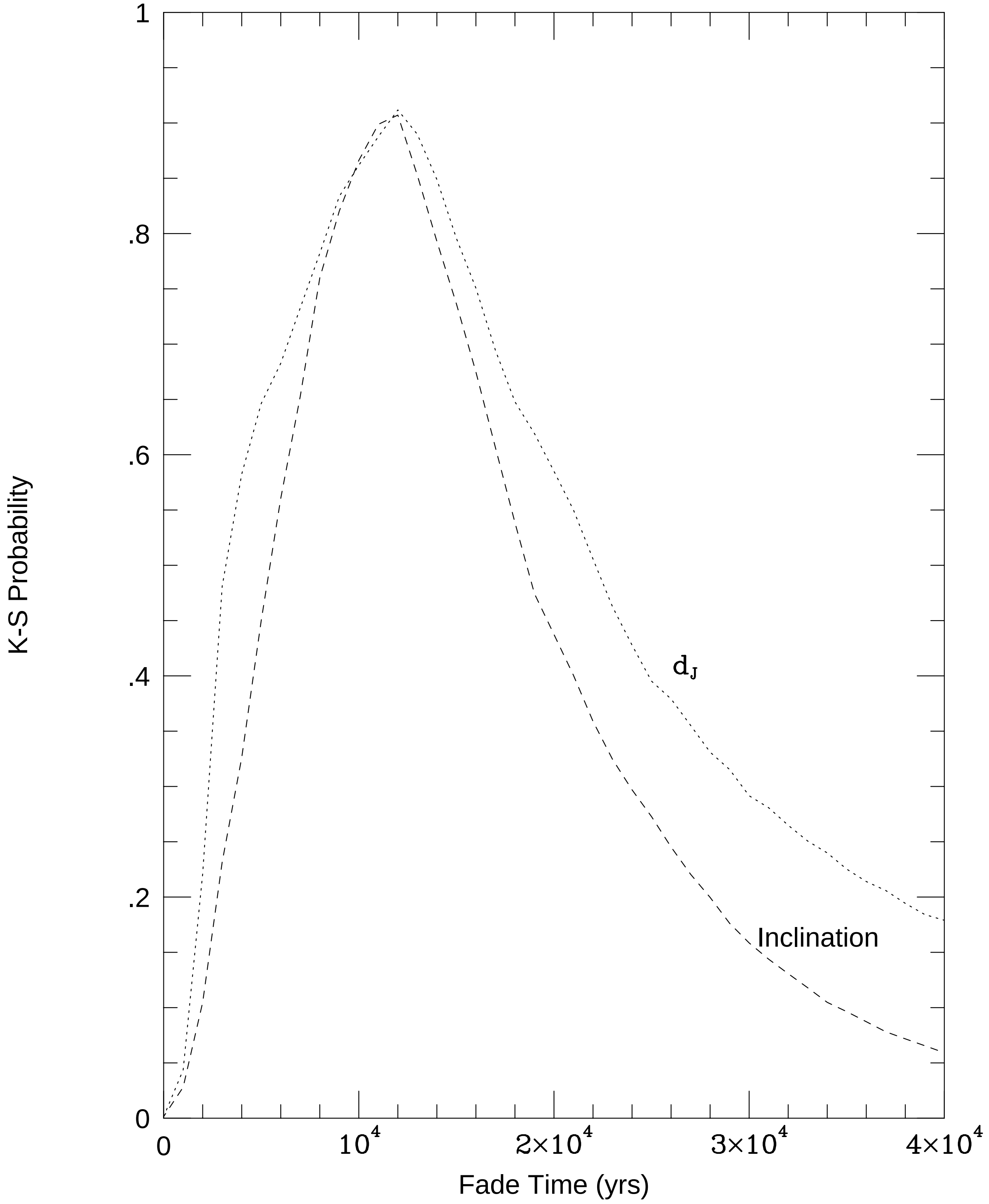

K-S Probability
1
.8
.6
.4
.2
0
0
10^4
2×10^4
3×10^4
4×10^4
Fade Time (yrs)
d_J
Inclination

FIGURE 11

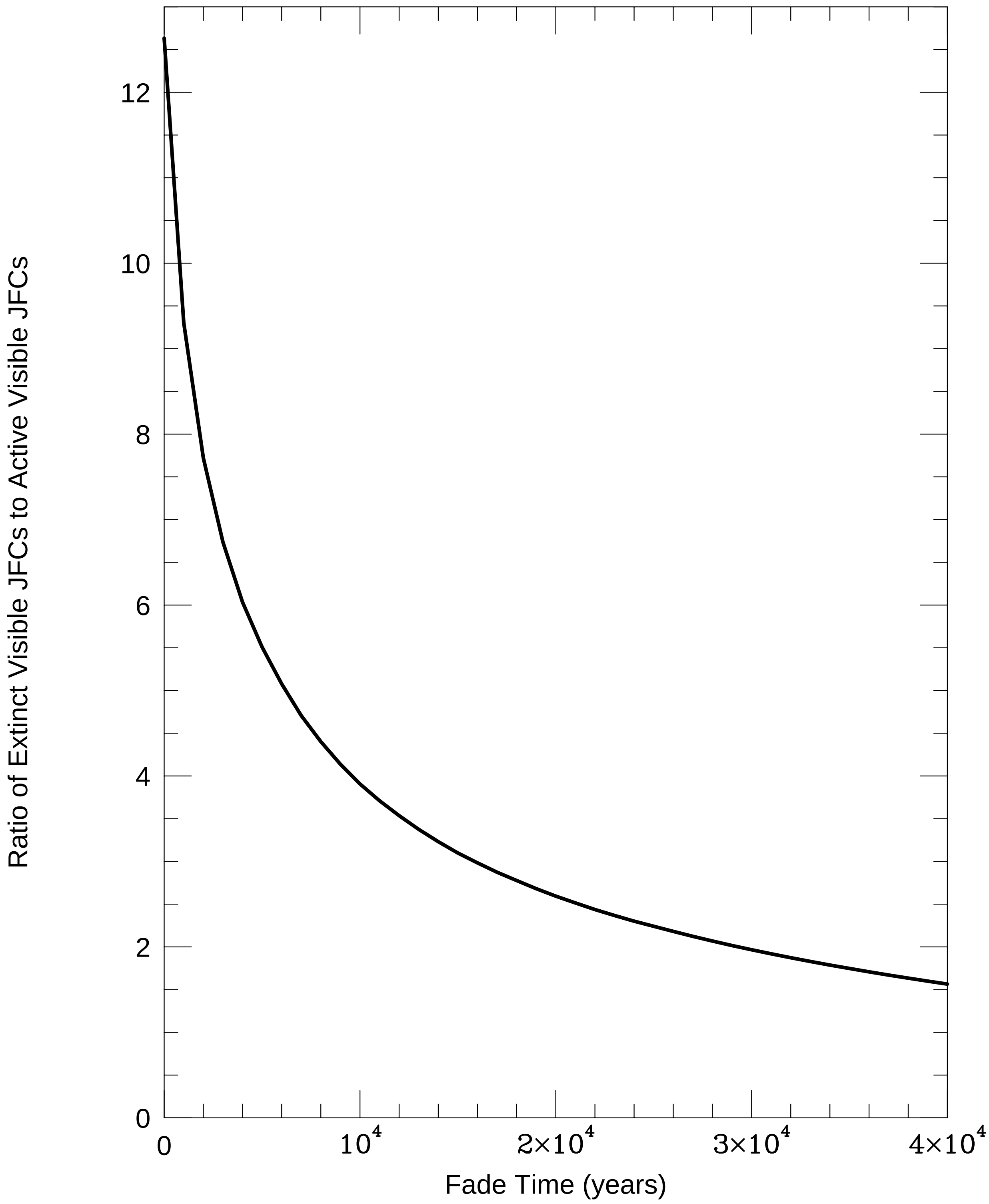

Ratio of Extinct Visible JFCs to Active Visible JFCs
0
2
4
6
8
10
12
0
10^4
2×10^4
3×10^4
4×10^4
Fade Time (years)

FIGURE 12

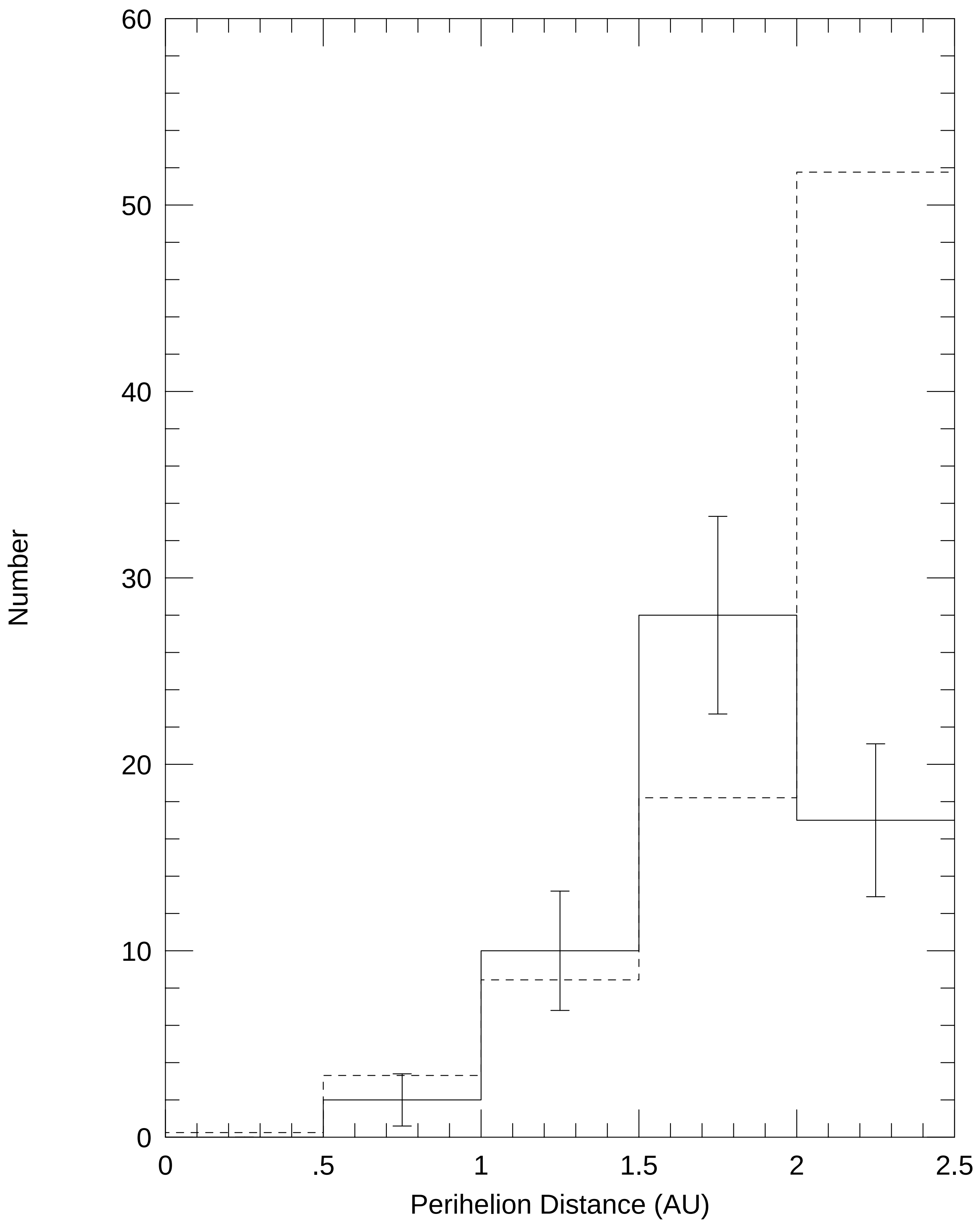

FIGURE 13

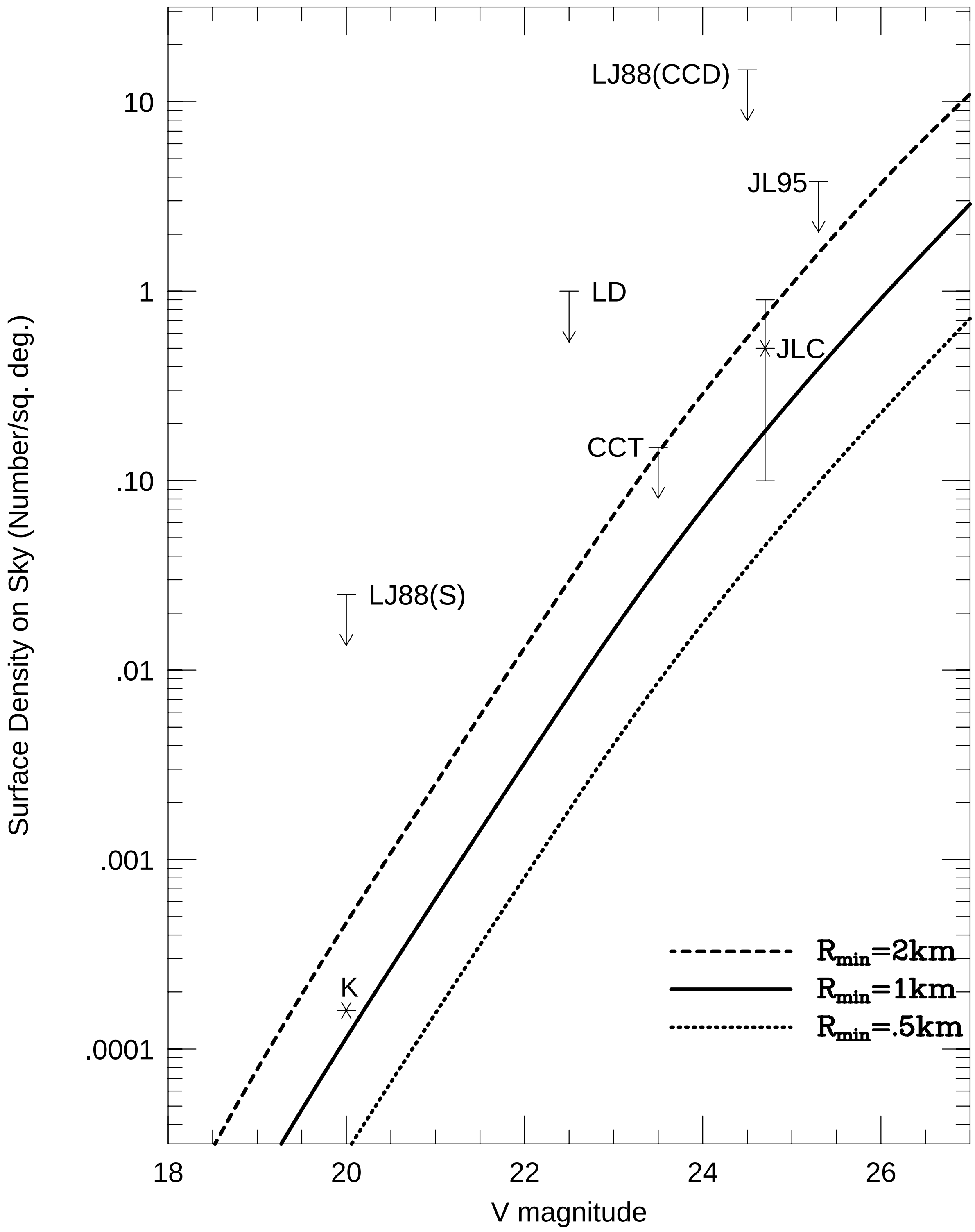

LJ88(CCD)
JL95
LD
JLC
CCT
LJ88(S)
K
R_{min}=2km
R_{min}=1km
R_{min}=.5km
10
1
.10
.01
.001
.0001
Surface Density on Sky (Number/sq. deg.)
18
20
22
24
26
V magnitude

FIGURE 14

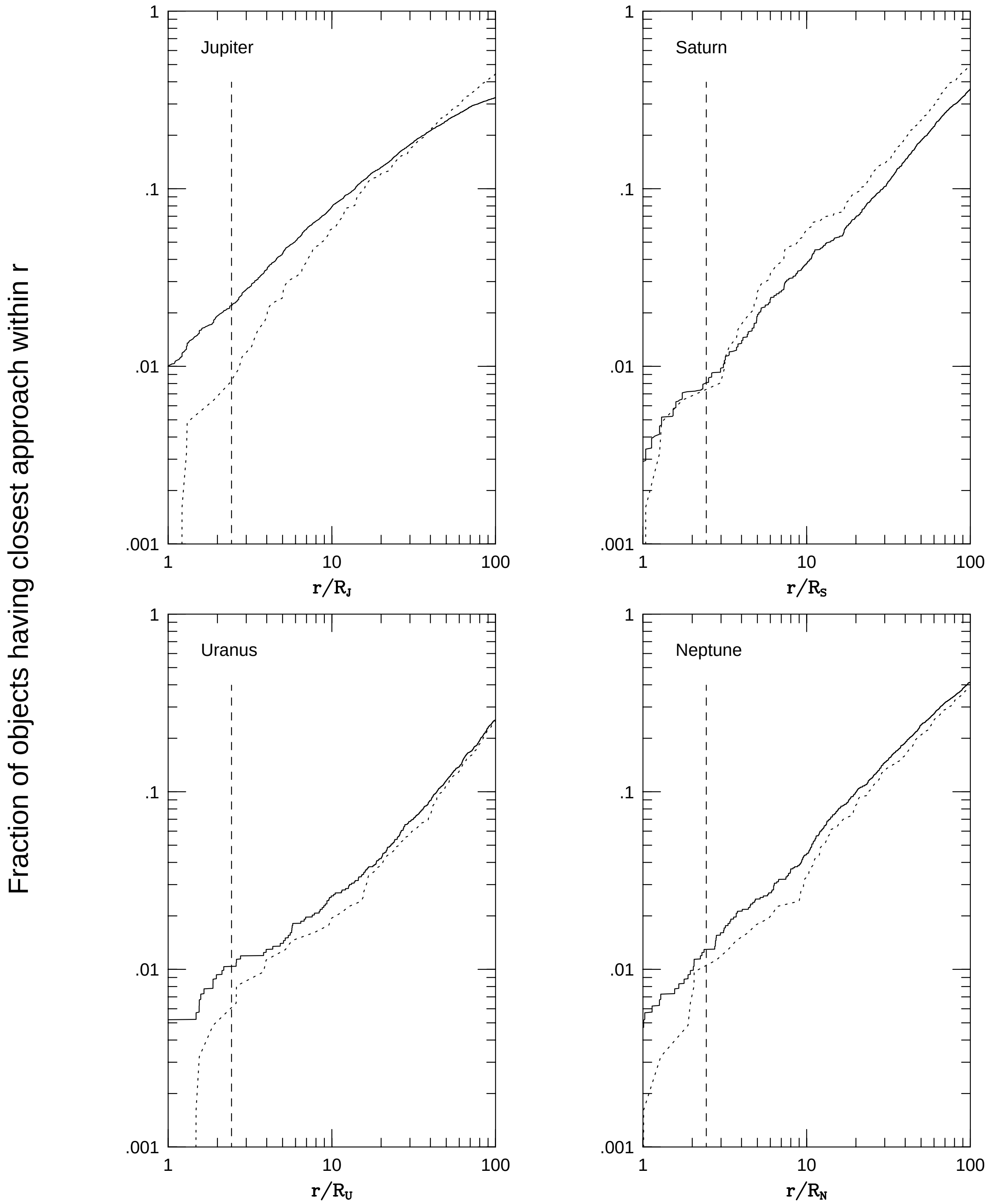
Fraction of objects having closest approach within r
Jupiter
Saturn
Uranus
Neptune
1
.1
.01
.001
1
10
100
r/R$_J$
r/R$_S$
r/R$_U$
r/R$_N$